Cooperative Beamforming for Reconfigurable Intelligent Surface-Assisted Symbiotic Radios

Hu Zhou , *Graduate Student Member, IEEE*, Xin Kang , *Senior Member, IEEE*,
Ying-Chang Liang , *Fellow, IEEE*, Sumei Sun , *Fellow, IEEE*, and Xuemin Shen , *Fellow, IEEE*

Abstract—In this paper, we study a novel reconfigurable intelligent surface (RIS) enabled symbiotic radio system, where a RIS is used to enhance the communication between the primary transmitter (PTx) and the primary receiver (PRx), and concurrently transmit its information (e.g., environmental monitoring information) to the PRx by varying the phase shifts. The objective is to cooperatively optimize the active transmit beamforming at the PTx and passive reflecting beamforming at the RIS to minimize the PTx's transmit power, subject to the signal-to-noise ratio constraints of primary and RIS transmissions. A new optimization problem is formulated where the RIS phase shifts are not only related to the channel state information (CSI), but also related to its message. First, we consider the perfect CSI setup to draw useful insights into the cooperative beamforming design between the PTx and RIS. Then, the worst-case robust beamforming design is carried out under the imperfect CSI setup. In particular, we take into account the imperfect successive interference cancellation at the PRx. Finally, simulation results show the effectiveness of the RIS information transfer and the integration of RIS into a symbiotic radio system can significantly improve the performance.

Index Terms—Cooperative beamforming, power minimization, reconfigurable intelligent surface, symbiotic radio.

I. INTRODUCTION

INTERNET-of-Things (IoT) has been envisioned as one of the key technologies for future wireless communications,

which covers a wide range of applications, ranging from smart transportation, smart home, smart grid, to smart agriculture, etc [2]. For the wide deployment of IoT devices, two critical challenges, i.e., the spectrum scarcity and energy supply issues, need to be solved. This is because spectrum resources left for IoT applications are limited since most of them have already been allocated to various radio systems. Moreover, it is of high cost to charge devices or replace batteries regularly. Therefore, such stringent challenges call for novel spectrum- and energy-efficient technologies for IoT networks [3].

One promising solution to the above challenges is *symbiotic radio* (SR) [2], [4], which originates from cooperative ambient backscatter communication (AmBC) [5]. A typical SR system consist of three nodes, namely, a *primary transmitter* (PTx), a *primary receiver* (PRx) and a *backscatter device* (BD) (e.g., tag and sensors). There are two types of transmission in the SR, i.e, the primary transmission and the BD transmission. Specifically, the BD transmits its message to the PRx by backscattering the incident signal emitted from the PTx, and thus the BD transmission shares the same spectrum and *radio frequency* (RF) source with primary transmission from the PTx to PRx. In return, the BD transmission provides additional multipath for the primary transmission. Therefore, the BD transmission and primary transmission form a mutually beneficial relationship from a spectrum sharing perspective [6]. Particularly, SR enables the BD to transmit its information by exploiting the backscatter communications, thus eliminating the need of power-hungry RF chains. There are some studies on SR systems. In [7], the sum-rate maximization and transmit power minimization problems were studied by optimizing the transmit beamforming vector at the PTx. In [8], the resource allocation strategies for the SR system were investigated under both long-term and short-term power constraints over fading states. While the SR topic is appealing and interesting, there still exists one fundamental challenge in the SR system. As the backscatter link consists of PTx-BD link and BD-PRx link, it suffers from double fading effect [5], resulting in that its strength is much weaker than that of the direct link. Thus, the performance of BD transmission is limited. Moreover, the BD may backscatter all the incident signals to PRx, which thus causes other interference at PRx.

Recently, *reconfigurable intelligent surface* (RIS), also known as *intelligent reflecting surface* (IRS) [9]–[13] has drawn considerable attention from both academia and industry for its ability to reconfigure the wireless propagation environment. Particularly, RIS is an artificial planar surface comprising a large number

of reflecting elements, each of which can apply a certain phase shift on the incident signal, and thus the reflected beams are formed towards desired directions (i.e, called passive reflecting beamforming). Owing to the appealing passive beamforming gain offered by RIS, the joint active and passive beamforming for RIS-assisted wireless communication systems have been extensively studied. Specifically, in [14], [15], RIS was used to minimize the total transmit power for *multi-user multiple-input-single-output* (MU-MISO) system. In [16], RIS was utilized to maximize the weighted sum-rate for MU-MISO system. RIS was also applied to physical layer security by studying a minimum-secrecy-rate maximization problem in [17]. It is also worth pointing out that most of the aforementioned studies on RIS are based on the assumption of perfect *channel state information* (CSI). However, it is challenging to obtain such perfect CSI in practice, especially in RIS-aided communication systems [18]–[20]. Under the assumption of imperfect CSI, robust beamforming for RIS-enhanced communication systems has also been investigated from different perspectives, such as transmit power minimization [21], [22], secure communication [23], [24], and cognitive radio networks [25].

Attracted by the above advantages of RIS, in this paper, we introduce RIS into the SR system, in which the RIS plays the role of a BD to simultaneously deliver its information and assist the primary transmission. The benefits brought by RIS are two-fold. First, by deploying a massive number of reflecting elements at the RIS, the RIS can bring the significant passive beamforming gain by collaboratively adjusting the phase shift of each element. It has been proved in [10], [14] that such beamforming gain is proportional to the square of the number of reflecting elements (i.e., N). Thus, we can increase N to compensate for the doubling fading effect of the backscatter link in the SR system. Second, RIS can also deliberately capture the signal coming from PTx via passive beamforming. Unlike most existing works on RIS which focus on assisting wireless links, once the phase shifts matrix is optimized, it is fixed. The RIS in our work has an additional function, i.e., delivering its own information. To achieve it, RIS needs to change the phase shifts periodically to transmit its information. For example, two phase states are needed to support the *binary phase shift keying* (BPSK) modulation. Denote the common RIS phase shifts by Θ. Then Θ is used to reflect signal for symbol '1,' and $-\Theta$ is used to reflect signal for symbol '−1'. The proposed RIS-assisted SR model is tailored for the IoT scenario, in which multiple sensors are embedded in the RIS. The sensors collect data from the environment, such as temperature, humidity, speed, etc. Then the RIS can feed back the sensors' data to the PRx by reflecting the signal coming from the PTx. In this way, the PRx can obtain the information both from RIS and PTx.

In this paper, we thoroughly investigate a RIS-assisted SR system under both perfect and imperfect CSI assumptions. The proposed model consists of a multi-antenna PTx, a RIS and a single-antenna PRx. The PTx communicates with PRx with the aid of RIS, at the same time, the RIS can send its message to PRx by varying the phase shifts. We are interested in the joint optimization of the active transmit beamforming at the PTx and the passive reflecting beamforming at the RIS to minimize the

PTx transmit power, subject to the *signal-to-noise ratio* (SNR) constraints of the primary transmission and the RIS transmission. It is worthy pointing out that the phase shifts of RIS are not only related to the CSI, but also related to its information to be transmitted, which brings a new challenge in the RIS passive beamforming design. Note that there were some works on RIS-assisted SR [26]–[28]. The authors of [26] and [27] studied the *bit error rate* (BER) minimization problem and the weighted sum-rate maximization problem by jointly optimizing the active and passive beamforming, respectively. The authors of [28] considered that the RIS simultaneously assists secure broadcasting and transmits its own signal, and formulated a minimum secrecy rate maximization problem. Different from the above works, this paper studies the power minimization problem for RIS-assisted SR, by considering both the perfect and imperfect CSI scenarios as well as both the continuous and discrete phase shift models. Moreover, the imperfect *successive interference cancellation* (SIC) effect at the PRx is also considered, which makes our study more challenging and more practical.

In a nutshell, the main contributions of our work are summarized as follows.

- We propose to integrate the RIS into the SR system to enhance the backscatter link while delivering RIS information. Then we formulate a novel joint active and passive beamforming design problem under both the perfect and imperfect CSI setups, subject to the SNR constraints of the primary and RIS transmissions.
- For the perfect CSI scenario, the formulated joint optimization problem is challenging to solve due to the coupled variables and non-convex constraints. We propose an efficient iterative algorithm to solve it. It is shown that RIS needs to align the backscatter link with the direct link.
- Furthermore, for the perfect CSI scenario, we analyze the impact of N (i.e., number of reflecting elements) on the PTx active beamforming to draw useful insights. It is shown that when N is small, the PTx needs to allocate more beam energy to the direct link. While N becomes larger, the PTx needs to allocate more beam energy to the backscatter link.
- For the imperfect CSI scenario, we take into account the effect of the imperfect SIC at the PRx, which makes the problem more challenging as compared to the perfect CSI scenario. To tackle these challenges, we first use the linear function model to characterize the impact of the imperfect SIC [29], [30]. Then the formulated robust beamforming problem is solved via the S-procedure and SDR technique.
- Finally, simulation results are provided to validate the effectiveness of the proposed algorithms and the superiority of the RIS-assisted SR system.

The rest of this paper is organized as follows. Section II outlines the system model and problem formulation. Section III studies the cooperative beamforming for the perfect CSI scenario. Section IV extends the cooperative beamforming strategy into the imperfect CSI scenario. Section V provides simulation results to evaluate the performance of our proposed algorithms. Finally, Section VI concludes our paper.
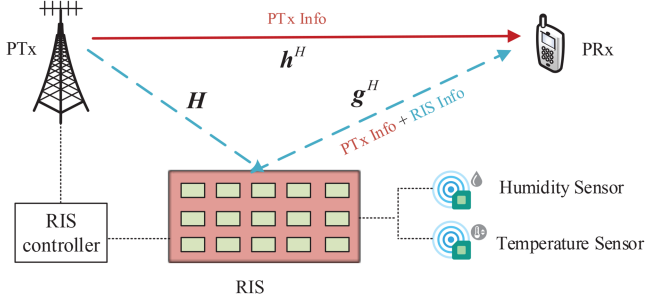
Fig. 1. System model of a RIS-assisted SR system: RIS simultaneously enhances primary transmission and transmits its own information to PRx via tuning the phase shifts.

Notations: Throughout this work, the scalars, vectors and matrices are denoted by the lower-case, boldface lower-case and boldface upper-case letters, i.e., $t, \boldsymbol{t}, \boldsymbol{T}$. $\mathbb{C}^{x \times y}$ denotes the space of $x \times y$ complex-valued matrices, and $\mathbb{S}^N$ represents the set of all N-dimensional real symmetric matrices. For a matrix $\boldsymbol{A}$, $\mathrm{tr}(\boldsymbol{A})$, $\mathrm{rank}(\boldsymbol{A})$, $\boldsymbol{A}^H$, $\boldsymbol{A}^T$, $\|\boldsymbol{A}\|_F$, $\mathrm{vec}(\boldsymbol{A})$ and $[\boldsymbol{A}]_{i,j}$ represent its trace, rank, conjugate transpose, transpose, Frobenius norm, a column vector by stacking all the elements and i-th row and j-th column element. For a vector $\boldsymbol{t}$, $\|\boldsymbol{t}\|_2$, $\boldsymbol{t}^H$, $[\boldsymbol{t}]_{end}$, $[\boldsymbol{t}]_{1:N}$ denote its Euclidean norm, conjugate transpose, the last element and the first N elements in the vector $\boldsymbol{t}$. $\mathbb{E}[\cdot]$ denotes statistical expectation. $\mathcal{CN}(\mu, \sigma^2)$ denotes *circularly symmetric complex Gaussian* (CSCG) distribution with mean μ and variance σ^2. $\boldsymbol{I}_N$ denotes the $N \times N$ identity matrix, and $\mathbf{1}_N = [1, \ldots, 1]^T$, and $\mathbf{0}_N = [0, \ldots, 0]^T$. $\boldsymbol{A} \succeq 0$ means $\boldsymbol{A}$ is a positive semi-definite matrix. $\boldsymbol{A} \otimes \boldsymbol{B}$ denotes the Kronecker products of $\boldsymbol{A}$ and $\boldsymbol{B}$. $\mathrm{blkdiag}(\boldsymbol{A}, \boldsymbol{B})$ denotes a block-diagonal matrix with $\boldsymbol{A}$ and $\boldsymbol{B}$ located on its main diagonal block. $\mathrm{diag}(\boldsymbol{t})$ represents a diagonal matrix whose diagonal elements are given by the vector $\boldsymbol{t}$. $|x|$, $\arg\{x\}$ and $\mathfrak{Re}\{x\}$ denotes the absolute value, phase and real part of a complex number x.

II. SYSTEM MODEL AND PROBLEM FORMULATION

As shown in Fig. 1, we consider a RIS-assisted SR system, which consists of a PTx with M antennas, a RIS with N reflecting elements, and a single-antenna PRx.[1] Particularly, the PTx communicates with PRx with the help of RIS, and the RIS sends its collected environmental information to the PRx by tuning its phase shifts. The RIS controller needs to send the information of RIS modulation scheme and its own minimum SNR requirement to the PTx. Then, the active and passive beamforming are jointly designed at the PTx based on the SNR requirements, and the PTx will send the optimized phase shifts to the RIS controller via a separate wireless control link [31]. In this section, we first present the channel model, followed by the signal transmission process in detail. After that, we introduce the channel uncertainty model. Finally, we present problem formulation under the perfect and imperfect CSI setups, respectively.

[1]For simplicity, we first consider a single-user case, but the proposed cooperative beamforming scheme can be extended to more general cases.

A. Channel Model

Without loss of generality, we make the same assumption as [14], [15], [32] on the RIS array deployment. We assume that a $M \times 1$ *uniform linear array* (ULA) is deployed at the PTx, and a $N = N_x \times N_y$ *uniform planar array* (UPA) is deployed at the RIS where N_x and N_y account for number of units in the horizontal and vertical directions, respectively. In this work, we consider block flat-fading channels, where the channel coefficients remain unchanged during one block, but may vary from one block to another. The channels from PTx to RIS, from PTx to PRx, and from RIS to PRx are denoted by $\boldsymbol{H} \in \mathbb{C}^{N \times M}$, $\boldsymbol{h}^H \in \mathbb{C}^{1 \times M}$, and $\boldsymbol{g}^H \in \mathbb{C}^{1 \times N}$, respectively. All the channels are composed of two parts: large-scale path loss and small-scale fading. Specifically, we model the distance-dependent large-scale path loss as

$$\mathrm{PL}(d, \alpha) = \beta_0 \left(\frac{d}{d_0} \right)^{-\alpha}, \tag{1}$$

where β_0 accounts for the path loss at the reference distance $d_0 = 1$ (m), α denotes the path loss exponent, and d denotes the distance in meters between arbitrary two nodes. Specifically, the distance between PTx and RIS, PTx and PRx, RIS and PRx, are denoted by d_1 (m), d_2 (m) and d_3 (m), respectively, and the corresponding path loss exponent are denoted by α_1, α_2, α_3, respectively. For the small-scale fading part, we assume it follows the Rician fading model. As a result, $\boldsymbol{H}$ can be modeled as [33]

$$\boldsymbol{H} = \sqrt{\mathrm{PL}(d_1, \alpha_1)} \left(\sqrt{\frac{\kappa_1}{\kappa_1 + 1}} \boldsymbol{H}^{LoS} + \sqrt{\frac{1}{\kappa_1 + 1}} \boldsymbol{H}^{NLoS} \right), \tag{2}$$

where κ_1 is the Rician factor, $\boldsymbol{H}^{LoS}$ and $\boldsymbol{H}^{NLoS}$ denote the *line-of-sight* (LoS) component and *non-LoS* (NLoS) component, respectively. Specifically, each element of $\boldsymbol{H}^{NLoS}$ is assumed to follow the CSCG distribution with zero mean and unit variance, i.e., $\mathcal{CN}(0, 1)$. $\boldsymbol{H}^{LoS}$ is modeled as

$$\boldsymbol{H}^{LoS} = \boldsymbol{a}_l \left(\vartheta_{TL}^A, \phi_{TL}^A \right) \boldsymbol{a}_t \left(\varphi_{TL}^D \right)^H, \tag{3}$$

where ϑ_{TL}^A and ϕ_{TL}^A are the azimuth and elevation *angle-of-arrival* (AoA) to the RIS, respectively; φ_{TL}^D denotes the *angle-of-departure* (AoD) from the PTx; $\boldsymbol{a}_l$ and $\boldsymbol{a}_t$ denote the steering vectors, which are expressed as [33]

$$\boldsymbol{a}_l(\vartheta_{TL}^A, \phi_{TL}^A) = f_{N_x}(-\cos(\phi_{TL}^A)\cos(\vartheta_{TL}^A)) \otimes$$
$$f_{N_y}(\cos(\phi_{TL}^A)\sin(\vartheta_{TL}^A)), \tag{4a}$$

$$\boldsymbol{a}_t(\varphi_{TL}^D) = f_M(\sin(\varphi_{TL}^D)), \tag{4b}$$

where $\otimes$ denotes the Kronecker product, and $f_K(u) = \left[1, e^{-j\frac{2\pi d_l}{\lambda_l}u}, \ldots, e^{-j\frac{2\pi d_l}{\lambda_l}(K-1)u} \right]^T$, λ_l denotes the carrier wavelength, and d_l denotes the antenna spacing. For simplicity, we set $d_l/\lambda_l = 1/2$, the same as in [33].
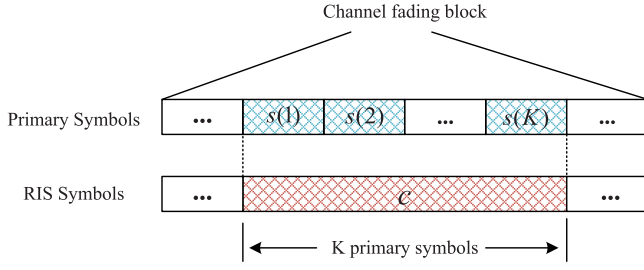
Fig. 2.   Transmission frame of the RIS-assisted symbiotic radio system.

Similarly, the channel responses $\boldsymbol{h}^H$ and $\boldsymbol{g}^H$ are modeled as

$$\boldsymbol{h}^H = \sqrt{\text{PL}\left(d_2, \alpha_2\right)} \left(\sqrt{\frac{\kappa_2}{\kappa_2 + 1}} \boldsymbol{h}^{LoS} + \sqrt{\frac{1}{\kappa_2 + 1}} \boldsymbol{h}^{NLoS} \right),$$
(5)

$$\boldsymbol{g}^H = \sqrt{\text{PL}\left(d_3, \alpha_3\right)} \left(\sqrt{\frac{\kappa_3}{\kappa_3 + 1}} \boldsymbol{g}^{LoS} + \sqrt{\frac{1}{\kappa_3 + 1}} \boldsymbol{g}^{NLoS} \right),$$
(6)

where κ_2 and κ_3 denote the Rician factors of $\boldsymbol{h}^H$ and $\boldsymbol{g}^H$, respectively. $\boldsymbol{h}^{LoS} = \boldsymbol{a}_t(\varphi_{TR}^D)^H$ and $\boldsymbol{g}^{LoS} = \boldsymbol{a}_l(\vartheta_{LR}^D, \phi_{LR}^D)^H$ denote the LoS components; φ_{TR}^D is the AoD from the PTx to the PRx; ϑ_{LR}^D and ϕ_{LR}^D are the corresponding azimuth and elevation AoD from the RIS to the PRx. Moreover, each element of $\boldsymbol{h}^{NLoS}$ and $\boldsymbol{g}^{NLoS}$ are assumed to follow the distribution of $\mathcal{CN}(0, 1)$, respectively.

B. Transmission Model

The transmission frame structure of the RIS-assisted SR system is shown in Fig. 2, we assume that one channel fading block covers several primary and RIS symbols. One RIS symbol covers K primary symbols, i.e., $T_c = KT_s$, where T_c and T_s are the period of RIS and primary symbols, respectively. Within one RIS symbol period of interest, one RIS symbol c and K primary symbols $[s(1), \ldots, s(K)]$ are transmitted.

Remark 1: Similar to the conventional backscatter communication [34], during the transmission phase, the PTx would first send the synchronization information (e.g., wake-up preamble) to the RIS controller via a wireless control link [31], then the RIS controller will decode the synchronization information and set the RIS into reflection state. Then, the PTx and the RIS can be synchronized.

1) Transmitted Signal At the PTx: Assume $s(k)$, where $k = 1, \ldots, K$, follows the CSCG distribution with zero mean and unit variance, i.e., $s(k) \sim \mathcal{CN}(0, 1)$. The PTx utilizes linear beamforming vector denoted by $\boldsymbol{w} \in \mathbb{C}^{M \times 1}$ to transmit its information, and PTx transmit power is defined as $p = \|\boldsymbol{w}\|^2$. Thus the transmitted signal at the PTx is given by $\boldsymbol{w}s(k)$, $k = 1, \ldots, K$.

2) Reflected Signal At the RIS: As aforementioned, we have $T_c = KT_s$, where K is an integer representing the spreading

gain [5]. BPSK modulation[2] is employed at the RIS, i.e., $c \in \{1, -1\}$. Denote a common phase shift matrix of RIS by $\boldsymbol{\Theta} = \text{diag}(e^{j\theta_1}, \ldots, e^{j\theta_N}) \in \mathbb{C}^{N \times N}$, then the reflection coefficients of RIS is given by $c\boldsymbol{\Theta}$. In other words, the RIS uses $\boldsymbol{\Theta}$ to reflect signal for symbol $c = 1$, and uses $-\boldsymbol{\Theta}$ to reflect signal for symbol $c = -1$. The reflected signal at the RIS can be expressed as $\boldsymbol{\Theta}\boldsymbol{H}\boldsymbol{w}s(k)c, k = 1, \ldots, K$.

In this paper, we consider both the continuous and discrete phase shift setups for the passive reflecting beamforming at the RIS.

- *Continuous phase shift:* the set of phase shifts is defined as

$$\mathcal{A}_1 \triangleq \{\theta | \theta \in [0, 2\pi)\}.$$
(7)

- *Discrete phase shift with b-bit resolutions:* the set of phase shifts is defined as

$$\mathcal{A}_2 \triangleq \left\{ \theta \middle| \theta \in \left\{ 0, \frac{2\pi}{2^b}, \ldots, \frac{2\pi}{2^b}(2^b - 1) \right\} \right\}.$$
(8)

3) Received Signal At the PRx: In the k-th symbol period of PTx signal, denote the received signal at the PRx by $y(k)$ for $k = 1, \ldots, K$, yielding

$$y(k) = \underbrace{\boldsymbol{h}^H \boldsymbol{w}s(k)}_{\text{Direct link}} + \underbrace{\boldsymbol{g}^H \boldsymbol{\Theta}\boldsymbol{H}\boldsymbol{w}s(k)c}_{\text{Backscatter link}} + z(k)$$

$$= \left(\boldsymbol{h}^H + \boldsymbol{g}^H \boldsymbol{\Theta}\boldsymbol{H}c\right) \boldsymbol{w}s(k) + z(k),$$
(9)

where $z(k)$ is the additive complex Gaussian noise with zero mean and variance σ^2, i.e., $z(k) \sim \mathcal{CN}(0, \sigma^2)$.

At the PRx, the information from the PTx and RIS are coupled together. To achieve highly reliable communication, PRx is designed to jointly decode the information from both the PTx and RIS [7]. Similar to [26], [28], we first decode the signal $s(k)$. The backscatter link can be viewed as multipath for primary transmission, and the average SNR of $s(k)$ needs to be taken expectation over c due to the uncertainty of c, yielding

$$\gamma_s = \mathbb{E}_c \left[\frac{1}{\sigma^2} \left| \left(\boldsymbol{h}^H + \boldsymbol{g}^H \boldsymbol{\Theta}\boldsymbol{H}c\right) \boldsymbol{w} \right|^2 \right]$$

$$= \frac{1}{2\sigma^2} \left[\left| \left(\boldsymbol{h}^H + \boldsymbol{g}^H \boldsymbol{\Theta}\boldsymbol{H}\right) \boldsymbol{w} \right|^2 + \left| \left(\boldsymbol{h}^H - \boldsymbol{g}^H \boldsymbol{\Theta}\boldsymbol{H}\right) \boldsymbol{w} \right|^2 \right],$$
(10)

where we assume the equal probability of $c = 1$ and $c = -1$.

After decoding $s(k), k = 1, \ldots, K$, the SIC technique is used to decode the RIS symbol c. To be specific, assuming $s(k)$ is perfectly decoded, we regenerate the signal from the direct link[3], i.e., $\boldsymbol{h}^H \boldsymbol{w}\boldsymbol{s}$, where $\boldsymbol{s} = [s(1), \ldots, s(K)]^T$. Then, we subtract it from the received signal vector $\boldsymbol{y} = [y(1), \ldots, y(K)]$ at the PRx. In practice, the perfect SIC is hard to realize due to the hardware

---

[2]We consider a simple yet practical binary modulation, which is easy for hardware implementation. When we extend to the higher-order modulation or new reflection pattern modulation, the proposed cooperative beamforming scheme is still applicable but needs some additional phase shifts design. This will be left for our future work.

[3]In the downlink training phase, the PTx sends pilots to the PRx while keeping the RIS off, then the received signal at the PRx is given by $y = \boldsymbol{h}^H \boldsymbol{w}s_p + z$, where s_p denotes the pilot, z denotes the additive Gaussian noise. Then the PRx can estimate $\boldsymbol{h}^H \boldsymbol{w}$ using the classical training-based estimation methods, e.g., least-square estimator.

impairments, which leads to imperfect SIC[4], i.e., there remains residual interference from the direct link. According to [29], a linear function model can effectively characterize the impact of imperfect SIC. This means the residual interference scales up linearly with the removed signal, and thus we have

$$\hat{y} = \underbrace{g^H \Theta H w s c}_{\text{Backscatter link signal}} + \underbrace{\delta h^H w s}_{\text{Residual intereference}} + \underbrace{z}_{\text{Noise}}, \quad (11)$$

where $\hat{y} = [\hat{y}_1, \ldots, \hat{y}_K]^T$ represents the signal after applying SIC; $z = [z(1), \ldots, z(K)]^T$ denotes the noise vector; δ ($0 \leq \delta \leq 1$) represents the SIC factor which measures the strength of the residual interference signal. $\delta = 0$ means perfect SIC, while $\delta = 1$ denotes no SIC is performed. The SIC factor is mainly affected by the hardware impairments, such as the phase noise of the local oscillator and in-phase /quadrature-phase (IQ) imbalances [36].

From (11), *maximum-ratio-combining* (MRC) is applied to decode c by treating the remaining part of the direct link signal as interference, and thus the *signal-to-interference-noise* (SINR) for decoding c can be approximated as (assuming $K \gg 1$)

$$\gamma_c = \frac{\left| g^H \Theta H w \right|^2}{\delta \left| h^H w \right|^2 + \frac{\sigma^2}{K}}, \quad (12)$$

where K is defined as $K = \frac{T_c}{T_s}$.

C. Transformation

For notation convenience, we let $v = [e^{j\theta_1}, \ldots, e^{j\theta_N}, 1]^H \in \mathbb{C}^{(N+1) \times 1}$, $G = \text{diag}(g^H) H$, $H_1 = \begin{bmatrix} G \\ h^H \end{bmatrix} \in \mathbb{C}^{(N+1) \times M}$, $H_2 = \begin{bmatrix} -G \\ h^H \end{bmatrix} \in \mathbb{C}^{(N+1) \times M}$, $H_3 = \begin{bmatrix} G \\ 0_M \end{bmatrix} \in \mathbb{C}^{(N+1) \times M}$, and $H_4 = \begin{bmatrix} 0_{N \times M} \\ h^H \end{bmatrix} \in \mathbb{C}^{(N+1) \times M}$, then the SNR expressions in (10) and (12) can be rewritten as

$$\gamma_s = \frac{1}{2\sigma^2} \left[\left| v^H H_1 w \right|^2 + \left| v^H H_2 w \right|^2 \right], \quad (13)$$

$$\gamma_c = \frac{\left| v^H H_3 w \right|^2}{\delta \left| v^H H_4 w \right|^2 + \frac{\sigma^2}{K}}. \quad (14)$$

D. Channel Uncertainty Model

In general, channel estimation is a pre-requisite for jointly optimizing the transmit beamforming vector w and the phase shifts θ. Currently, several efficient algorithms have been designed to estimate the cascaded channel, i.e., the channel spanning from the PTx to the PRx via the RIS, by switching on all the reflecting elements. For instance, in [37], the RIS-related CSI is estimated by minimizing the Cramer-Rao lower bound. In [18], the *compressive sensing* (CS) technique was utilized to perform channel estimation by leveraging the sparsity of cascaded channels.

In this work, we assume the direct channel h and cascaded channel G are estimated by using the channel estimation approach in [37]. Due to the imperfect CSI which may be caused by noise, limited training, outdated feedback and quantization error [38], we assume that the exact channels lie in the vicinity of estimated channels. As a result, the uncertainty model can be expressed as

$$G = \widetilde{G} + \Delta G, \quad (15)$$

$$h = \widetilde{h} + \Delta h, \quad (16)$$

where $\widetilde{G}$ and $\widetilde{h}$ account for the estimated channels, ΔG and Δh denote the CSI errors. The CSI errors are assumed to be bounded in the spherical regions[5] as follows

$$\mathcal{U}_g \triangleq \left\{ \Delta G \in \mathbb{C}^{N \times M} : \|\Delta G\|_F \leq \varepsilon_g \right\}, \quad (17)$$

$$\mathcal{U}_h \triangleq \left\{ \Delta h \in \mathbb{C}^{M \times 1} : \|\Delta h\|_2 \leq \varepsilon_h \right\}, \quad (18)$$

where ε_g and ε_h are the radius of the bounded regions known by the PTx. In terms of [21], [41], channel uncertainty ratios are used to describe a certain amount of channel uncertainties. By controlling the corresponding ratios denoted by ϵ_g and ϵ_h, different channel uncertainties can be calculated as $\varepsilon_g = \epsilon_g \|\widetilde{G}\|_F$, $\varepsilon_h = \epsilon_h \|\widetilde{h}\|_2$, where $\epsilon_g, \epsilon_h \in [0, 1]$.

E. Problem Formulation

In this paper, we target at minimizing the transmit power at the PTx via jointly optimizing the primary beamforming vector w and the phase shifts θ subject to the SNR constraints of the PTx and RIS transmissions. Particularly, both the perfect CSI and imperfect CSI scenarios are considered.

1) Perfect CSI Case: To draw valuable insights into the cooperative beamforming design, we first consider an ideal case with the assumption of perfect CSI and perfect SIC. In this case, CSI errors equal to zero, i.e., $\Delta G = 0_{N \times M}$, $\Delta h = 0_M$. Optimization results for the perfect CSI scenario can serve as a performance upper bound for studying the imperfect CSI scenario. Consequently, the problem can be formulated as

$$\underline{\textbf{P1}} : \quad \min_{w, \theta} \|w\|^2 \quad (19a)$$

$$\text{s.t. } \gamma_s \geq \Gamma_s, \quad (19b)$$

$$\gamma_c \geq \Gamma_c, \text{with } \delta = 0, \quad (19c)$$

$$\theta_n \in \mathcal{A}, \forall n = 1, \ldots, N, \quad (19d)$$

where Γ_s and Γ_c denote the minimum SNR requirements for the primary transmission and the RIS transmission, respectively. $\mathcal{A}$ represents $\mathcal{A}_1$ (given by (7)) for the continuous phase shift case or $\mathcal{A}_2$ (given by (8)) for the discrete phase shift case. Note that in (19c), $\delta = 0$, and thus *left-hand-side* (LHS) of (19c) is reduced to $\gamma_c = \frac{K |g^H \Theta H w|^2}{\sigma^2}$.

---

[4]In practice, the exact modeling of SIC is very complicated. For the theoretical study, there are two approaches to deal with the SIC, one is to assume perfect SIC to seek a performance upperbound [7], [26], while the other is to use a linear model to characterize the effect of imperfect SIC [29], [35]. Thus, to facilitate theoretical analysis, we also adopt these approaches in our work.

[5]Probabilistic CSI error model [39] and bounded CSI error model [40] are both two approaches for the robust design, which focus on the average performance and the worst-case performance, respectively. In this paper, we adopt the bounded CSI error model. Note that the probabilistic CSI error model is also quite important when we focus on the average performance of the system and is worthy of future investigation.

2) Imperfect CSI Case: Considering the practical case where the perfect CSI is hard to obtain, we aim to study the joint robust beamforming design of the RIS-assisted SR system under the imperfect CSI setup. In particular, the imperfect SIC at the PRx is taken into account. The power minimization problem is formulated as

$$\underline{\textbf{P2}}: \quad \min_{\boldsymbol{w},\boldsymbol{\theta}} \|\boldsymbol{w}\|^2 \tag{20a}$$

$$\text{s.t. } \gamma_s \geq \Gamma_s, \tag{20b}$$

$$\gamma_c \geq \Gamma_c \text{ with } \delta \neq 0, \tag{20c}$$

$$\theta_n \in \mathcal{A}, \forall n = 1, \ldots, N, \tag{20d}$$

$$\Delta \boldsymbol{G} \in \mathcal{U}_g, \tag{20e}$$

$$\Delta \boldsymbol{h} \in \mathcal{U}_h. \tag{20f}$$

Compared with P1, the additional constraints (20e) and (20f) in P2 represent the norm-based uncertainty sets. This means that the SNR constraints (20b), (20c) must hold for all possible CSI errors that belong to the uncertainty sets. It is worth pointing out that imperfect SIC is implemented for this practical case. Thus, the γ_s and γ_c are different from those in P1.

III. COOPERATIVE BEAMFORMING DESIGN FOR PERFECT CSI CASE

In this section, we present the solution to P1. Actually, P1 is non-convex due to its non-convex constraints, and even worse, $\boldsymbol{w}$ and $\boldsymbol{\theta}$ are highly coupled with each other. *Alternating optimization* (AO) algorithm [14] has been widely used to solve such coupled non-convex problems. Its basic idea is to decouple the original problem into several subproblems, and then solve them iteratively. As for the non-convex P1, we decouple it into two subproblems. One is related to active transmit beamforming, while the other is related to the passive beamforming, given by

$$\underline{\textbf{P1-A}}: \quad \min_{\boldsymbol{w}} \|\boldsymbol{w}\|^2 \tag{21a}$$

$$\text{s.t. } (19b), (19c), \tag{21b}$$

and

$$\underline{\textbf{P1-B}}: \quad \min_{\boldsymbol{\theta}} \|\boldsymbol{w}\|^2 \tag{22a}$$

$$\text{s.t. } (19b), (19c), (19d). \tag{22b}$$

A. Active Transmit Beamforming

In the l-th iteration, given the phase shifts $\boldsymbol{\theta}^{(l-1)}$, the original problem P1 is reduced to the active beamforming-associated problem P1-A. The PTx needs to design the its beamforming vector $\boldsymbol{w}$ to support the primary and RIS transmissions. As we know, the PTx communicates with PRx through the PTx-PRx link (i.e., $\boldsymbol{h}$) and PTx-RIS-PRx link (i.e., $\boldsymbol{f} \triangleq (\boldsymbol{g}^H \boldsymbol{\Theta} \boldsymbol{H})^H$). Therefore, the PTx should beam towards the two links to support the RIS-assisted SR system. Denote the normalized direct channel and backscatter channel by $\overline{\boldsymbol{h}} = \frac{\boldsymbol{h}}{\|\boldsymbol{h}\|}, \overline{\boldsymbol{f}} = \frac{\boldsymbol{f}}{\|\boldsymbol{f}\|}$, respectively. We have the following proposition.

Proposition 1: The optimal beamforming vector $\boldsymbol{w}^\star$ is written in the form as $\boldsymbol{w}^\star = a_1 \overline{\boldsymbol{h}} + a_2 \overline{\boldsymbol{f}}$, where a_1 and a_2 represent the complex weights.

Proof: The proof is similar to [7, Proposition 3], and thus omitted here for brevity. ∎

Proposition 1 shows that the optimal transmit beamforming vector lies in the space spanned by the normalized direct channel $\overline{\boldsymbol{h}}$ and the normalized backscatter channel $\overline{\boldsymbol{f}}$. In particular, the $\frac{|a_1|^2}{\|\boldsymbol{w}^\star\|^2}$ denotes the fraction of beam energy allocated to the direct link, while the $\frac{|a_2|^2}{\|\boldsymbol{w}^\star\|^2}$ denotes the fraction of beam energy allocated to the backscatter link.

From Proposition 1, the transmit beamforming vector is written as

$$\boldsymbol{w} = a_1 \overline{\boldsymbol{h}} + a_2 \overline{\boldsymbol{f}} = \boldsymbol{D}\boldsymbol{a}, \tag{23}$$

where $\boldsymbol{D} = [\overline{\boldsymbol{h}}, \overline{\boldsymbol{f}}] \in \mathbb{C}^{M \times 2}$, $\boldsymbol{a} = [a_1, a_2]^T \in \mathbb{C}^{2 \times 1}$. It can be seen that optimizing the beamforming vector $\boldsymbol{w}$ is equivalent to optimizing the complex weight vector $\boldsymbol{a}$. With the Proposition 1, we introduce two *positive semi-definite* (PSD) matrices $\boldsymbol{A} = \boldsymbol{a}\boldsymbol{a}^H$, $\boldsymbol{V} = \boldsymbol{v}\boldsymbol{v}^H$, which satisfy $\boldsymbol{A} \succeq 0$, $\boldsymbol{V} \succeq 0$, and $\text{rank}(\boldsymbol{A}) = 1$, $\text{rank}(\boldsymbol{V}) = 1$. Denote $\boldsymbol{S}_1 = (\boldsymbol{H}_1 \boldsymbol{D})^H \boldsymbol{V} \boldsymbol{H}_1 \boldsymbol{D}$, $\boldsymbol{S}_2 = (\boldsymbol{H}_2 \boldsymbol{D})^H \boldsymbol{V} \boldsymbol{H}_2 \boldsymbol{D}, \boldsymbol{S}_3 = (\boldsymbol{H}_3 \boldsymbol{D})^H \boldsymbol{V} \boldsymbol{H}_3 \boldsymbol{D}$, the problem P1-A can be rewritten as

$$\underline{\textbf{P1-A1}}: \quad \min_{\boldsymbol{A}} \text{tr}(\boldsymbol{D}^H \boldsymbol{D} \boldsymbol{A}) \tag{24a}$$

$$\text{s.t. } \frac{1}{2\sigma^2} \left(\text{tr}(\boldsymbol{S}_1 \boldsymbol{A}) + \text{tr}(\boldsymbol{S}_2 \boldsymbol{A}) \right) \geq \Gamma_s, \tag{24b}$$

$$\frac{K}{\sigma^2} \text{tr}(\boldsymbol{S}_3 \boldsymbol{A}) \geq \Gamma_c, \tag{24c}$$

$$\boldsymbol{A} \succeq 0, \tag{24d}$$

$$\text{rank}(\boldsymbol{A}) = 1. \tag{24e}$$

For P1-A1, the semi-definite constraints (24b), (24c), (24d) are convex, however, the rank-one constraint (24e) is non-convex. We resort to the SDR technique by relaxing the rank-one constraint, yielding

$$\underline{\textbf{P1-A2}}: \quad \min_{\boldsymbol{A}} \text{tr}(\boldsymbol{D}^H \boldsymbol{D} \boldsymbol{A}) \tag{25a}$$

$$\text{s.t. } (24b), (24c), (24d). \tag{25b}$$

The relaxation problem P1-A2 is a convex *semi-definite programming* (SDP) problem, and thus it can be efficiently solved by optimization tools, such as CVX [42]. In general, the optimal solution $\boldsymbol{A}^\star$ is not a rank-one matrix. However, for our specific problem P1-A2, it is shown that optimal solution $\boldsymbol{A}^\star$ is of rank-one, yielding the following property.

Proposition 2: The optimal solution $\boldsymbol{A}^\star$ to P1-A2 always satisfies $\text{rank}(\boldsymbol{A}^\star) = 1$.

Proof: Please refer to Appendix A. ∎

Based on the Proposition 2, it shows that the rank-one constraint relaxation is tight. We can thus obtain a globally optimal solution to P1-A1 by solving P1-A2. Then, we can further obtain the optimal transmit beamforming vector $\boldsymbol{w}^\star$ by decomposing $\boldsymbol{A}^\star$. To be specific, we first conduct $\boldsymbol{A}^\star$ as $\boldsymbol{A}^\star = \boldsymbol{U}_w \boldsymbol{\Sigma}_w \boldsymbol{U}_w^H$, where $\boldsymbol{U}_w = [\boldsymbol{u}_1, \ldots, \boldsymbol{u}_M] \in \mathbb{C}^{M \times M}$ and $\boldsymbol{\Sigma}_w \in \mathbb{C}^{M \times M}$ are a

unitary matrix and a diagonal matrix whose diagonal elements are the singular value of $A^\star$, respectively, then $a^\star$ is calculated as $a^\star = \sqrt{[\Sigma_w]_{1,1}}u_1$. Finally, the optimal beamforming vector is given by $w^\star = Da^\star$.

In the RIS-assisted SR system, the PTx transmit beamforming needs to support both the primary and RIS transmissions, Proposition 1 suggests that the PTx should beam towards the direct link and backscatter link. To obtain essential insights into the RIS-assisted SR system, we analyze the impact of the number of reflecting elements (i.e., N) on the PTx transmit beamforming. Note that the SNR of primary transmission ($\frac{1}{2\sigma^2}[|(h^H + g^H\Theta H)w|^2 + |(h^H - g^H\Theta H)w|^2] = \frac{1}{\sigma^2}(|h^Hw|^2 + |g^H\Theta Hw|^2)$) is related to direct link and the backscatter link, while the SNR of RIS transmission ($\frac{K|g^H\Theta Hw|^2}{\sigma^2}$) is only related to backscatter link.

Remark 2: The PTx transmit beamforming depends on the strength of the direct link and the backscatter link. To be specific, when the number of reflecting elements (i.e., N) is small, the strength of backscatter link is much weaker than that of the direct link. In this situation, the PTx would like to allocate more beam energy $\frac{|a_1|^2}{\|w^\star\|^2}$ to the direct link to satisfy the SNR requirement (i.e., Γ_s) of primary transmission, at the same time, the PTx must allocate a certain amount of beam energy $\frac{|a_2|^2}{\|w^\star\|^2}$ to the backscatter link to guarantee the lower SNR requirement (i.e., Γ_c) of the RIS transmission. As $N \to \infty$, the backscatter link would be much stronger than the direct link due to the passive beamforming gain, the impact of the direct link can be ignored. The PTx would like to allocate almost all its beam energy to the backscatter link to meet the SNR requirement of primary transmission, meanwhile, reliable RIS transmission can also be achieved.

B. Passive Beamforming With Continuous Phase Shifts

In the l-th iteration, given $w^{(l)}$ and $\theta^{(l-1)}$, then we optimize the phase shifts θ. Notice that P1-B is a feasibility checking problem since the objective function does not involve the variable θ. For a feasible solution θ to P1-B, it remains unknown whether the transmit power $\|w\|^2$ in P1-A will decrease or not, and the convergence of P1 can not be guaranteed. According to [14], it is intuitive that minimum transmit power will decrease if the feasible solution to P1-B achieves higher performance metrics than the requirements, i.e., $\gamma_s \geq \Gamma_s$ and $\gamma_c \geq \Gamma_c$. To this end, we aim to maximize the sum of the ratio of primary transmission SNR to its required SNR and the ratio of RIS transmission SNR to its required SNR (i.e., $\frac{\gamma_s}{\Gamma_s} + \frac{\gamma_c}{\Gamma_c}$) without violating original constraints. As a result, P1-B is transformed into the following problem.

$$\textbf{P1} - \textbf{B1}: \quad \max_{\theta} \quad \frac{\gamma_s}{\Gamma_s} + \frac{\gamma_c}{\Gamma_c} \tag{26a}$$

$$\text{s.t. (19b), (19c), (19d).} \tag{26b}$$

Although the problem P1-B1 is non-convex with respect to θ, there exists a closed-form solution to the above problem by exploiting the structure of the objective function of P1-B1. We define $\zeta_1(\theta) = \gamma_s$, $\zeta_2(\theta) = \gamma_c$, where γ_s and γ_c are given in (10) and (12), respectively. Then the objective function in P1-B1

can be rewritten as $\frac{\zeta_1(\theta)}{\Gamma_s} + \frac{\zeta_2(\theta)}{\Gamma_c}$. First, we derive the maximum value of $\zeta_1(\theta)$. Denote $\psi = h^Hw$, $z = \text{diag}(g^H)Hw$, we have

$$\zeta_1(\theta) \overset{a}{=} \frac{1}{2\sigma^2}\left||\psi| + \sum_{i=1}^{N}|z_i|e^{j\eta_i}\right|^2 + \frac{1}{2\sigma^2}\left||\psi| + \sum_{i=1}^{N}|z_i|e^{j(\eta_i+\pi)}\right|^2$$

$$\overset{b}{=} \frac{1}{\sigma^2}\left(\widetilde{\psi} + 2\sum_{i=1}^{N-1}\sum_{j=i+1}^{N}|z_i||z_j|\cos(\eta_i - \eta_j)\right)$$

$$\overset{c}{\leq} \frac{1}{\sigma^2}\left(\widetilde{\psi} + 2\sum_{i=1}^{N-1}\sum_{j=i+1}^{N}|z_i||z_j|\right), \tag{27}$$

where "a" and "b" follow from $\eta_i \triangleq \theta_i + \arg(z_i) - \arg(\psi)$ and $\widetilde{\psi} \triangleq |\psi|^2 + \sum_{i=1}^{N}|z_i|^2$, respectively. For "$c$," it is obvious that $\zeta_1(\theta)$ achieves its maximum value iff $\eta_i = \eta_j = \varrho_1, \forall i,j = 1,\ldots,N$, where ϱ_1 is an arbitrary constant phase. Then, according to the previous definitions, we have $\theta_i = \varrho_1 + \arg(\psi) - \arg(z_i), \forall i = 1,\ldots,N$. Next, we derive the maximum value of $\zeta_2(\theta)$ with respect to θ.

$$\zeta_2(\theta) = \frac{K}{\sigma^2}\left|\sum_{i=1}^{N}|z_i|e^{j(\theta_i+\arg(z_i))}\right|^2 \overset{d}{\leq} \frac{K}{\sigma^2}\left|\sum_{i=1}^{N}|z_i|\right|^2, \tag{28}$$

based on the triangle inequality, "d" holds iff $\theta_i + \arg(z_i) = \varrho_2$, where ϱ_2 is a constant phase. It is interesting to observe that if we set $\varrho_1 = -\arg(\psi)$, $\varrho_2 = 0$, then the phase shifts of RIS are given by

$$\theta_i^\star = -\arg(z_i), \forall i = 1,\ldots,N. \tag{29}$$

Note that the above phase shifts are capable of maximizing the objective function of P1-B1, then we need to check whether the above phase shifts satisfy the constraints (19b), (19c). Denote the closed-form solution $\{\theta_i^\star\}_{i=1}^{N}$ by $\theta^{(l)}$, it is easy to verify that

$$\gamma_s(w^{(l)}; \theta^{(l)}) \geq \gamma_s(w^{(l)}; \theta^{(l-1)}) \geq \Gamma_s, \tag{30}$$

$$\gamma_c(w^{(l)}; \theta^{(l)}) \geq \gamma_c(w^{(l)}; \theta^{(l-1)}) \geq \Gamma_c. \tag{31}$$

Thus, we claim that phase shifts $\{\theta_i^\star\}_{i=1}^{N}$ in (29) are the globally optimal solutions to P1-B1, yielding the following theorem.

Theorem 1: In the l-th iteration, the closed-form solution to P1-B1 is $\theta_n^{(l)} = -\arg(z_n), \forall n = 1,\ldots,N$, where $z = \text{diag}(g^H)Hw$.

When the closed-form solution is obtained, we construct $V^{(l)}$ using $v = [e^{j\theta_1^{(l)}}, \ldots, e^{j\theta_N^{(l)}}, 1]^H$, then substitute it to the subproblem P1-A1. Then the two subproblems, i.e., P1-A1 and P1-B1 are solved iteratively until convergence.

From Theorem 1, the term $z = \text{diag}(g^H)Hw$ is the product of the RIS-PRx link, PTx-RIS link and the transmit beamforming vector, where Hw can be regarded as the effective PTx-RIS link, and $\text{diag}(g^H)$ is regarded as the effective RIS-PRx link. Hence, the closed-form solution shown in Theorem 1 suggests that RIS phase shifts should be tuned to align the effective PTx-RIS link and effective RIS-PRx link, such that the SNR of RIS transmission associated with backscatter link ($\frac{K|g^H\Theta Hw|^2}{\sigma^2}$) can be maximized. As for the primary

transmission, its SNR is written as $\frac{1}{2\sigma^2}[|(\boldsymbol{h}^H + \boldsymbol{g}^H \boldsymbol{\Theta} \boldsymbol{H})\boldsymbol{w}|^2 + |(\boldsymbol{h}^H - \boldsymbol{g}^H \boldsymbol{\Theta} \boldsymbol{H})\boldsymbol{w}|^2] = \frac{1}{\sigma^2}(|\boldsymbol{h}^H \boldsymbol{w}|^2 + |\boldsymbol{g}^H \boldsymbol{\Theta} \boldsymbol{H} \boldsymbol{w}|^2)$. It is interesting to find that for its simplified form, the SNR of primary transmission can be maximized by enhancing the backscatter link. Therefore, the closed-form solution are capable of enhancing both the primary and RIS transmissions.

C. Passive Beamforming With Discrete Phase Shifts

In the above subsection, we investigate the continuous phase shifts design. However, it is difficult to tune the phase shifts continuously in practice due to the hardware limitation. Thus, we study the discrete phase shifts design problem in this subsection. According to [15], when a large number of reflecting elements are equipped at the RIS, it is much more cost-effective to configure the phase shifts with a small number of bits. Therefore, we first study the 1-bit phase shifter design problem.

1) Phase Shifter With 1-Bit Resolution: Similar to P1-B1, in the l-th iteration, given $\boldsymbol{w}^{(l)}$ and $\boldsymbol{\theta}^{(l-1)}$, we have the following phase shifts optimization problem

$$\underline{\textbf{P1-B2}}: \quad \min_{\boldsymbol{\theta}} \ \|\boldsymbol{w}\|^2 \tag{32a}$$

$$\text{s.t.} \quad ((19b), (19c),$$

$$\theta_n \in \{0, \pi\}, \forall n = 1, \dots, N. \tag{32b}$$

Since the optimization variable $\boldsymbol{\theta}$ is implicit in P1-B2, we need to provide more tractable expressions of the constraints in P1-B2. Recall the variable $\boldsymbol{V}$ defined in Section III-A, we denote $\boldsymbol{B}_1 = \boldsymbol{H}_1 \boldsymbol{w}(\boldsymbol{H}_1 \boldsymbol{w})^H \in \mathbb{C}^{(N+1) \times (N+1)}$, $\boldsymbol{B}_2 = \boldsymbol{H}_2 \boldsymbol{w}(\boldsymbol{H}_2 \boldsymbol{w})^H \in \mathbb{C}^{(N+1) \times (N+1)}$, and $\boldsymbol{B}_3 = \boldsymbol{H}_3 \boldsymbol{w}(\boldsymbol{H}_3 \boldsymbol{w})^H \in \mathbb{C}^{(N+1) \times (N+1)}$, then we have

$$\left| \boldsymbol{v}^H \boldsymbol{H}_k \boldsymbol{w} \right|^2 = \boldsymbol{v}^H \boldsymbol{B}_k \boldsymbol{v} = \text{tr}(\boldsymbol{B}_k \boldsymbol{V}), \ k = 1, 2, 3. \tag{33}$$

Accordingly, γ_s in (13) and γ_c in (14) can be rewritten as

$$\gamma_s(\boldsymbol{V}) = \frac{1}{2\sigma^2} \left[\text{tr}(\boldsymbol{B}_1 \boldsymbol{V}) + \text{tr}(\boldsymbol{B}_2 \boldsymbol{V}) \right], \tag{34}$$

$$\gamma_c(\boldsymbol{V}) = \frac{K}{\sigma^2} \text{tr}(\boldsymbol{B}_3 \boldsymbol{V}). \tag{35}$$

Then P1-B2 can be transformed to

$$\underline{\textbf{P1-B3}}: \quad \min_{\boldsymbol{V}} \ \|\boldsymbol{w}\|^2$$

$$\text{s.t.} \ \gamma_s(\boldsymbol{V}) \geq \Gamma_s, \tag{36a}$$

$$\gamma_c(\boldsymbol{V}) \geq \Gamma_c, \tag{36b}$$

$$\text{rank}(\boldsymbol{V}) = 1, \tag{36c}$$

$$[\boldsymbol{V}]_{n,n} = 1, \forall n = 1, \dots, N+1. \tag{36d}$$

Note that P1-B3 is a feasibility testing problem. Same as P1-B1, if the obtained feasible solution can achieve higher performance values (i.e., γ_s and γ_c) than the SNR constraints (i.e., Γ_s and Γ_c), the minimum transmit power will decrease, and thus the convergence of P1 can be guaranteed. Then, we introduce a slack variable t, which satisfies $t \geq 1$, P1-B3 can be rewritten as

$$\underline{\textbf{P1-B4}}: \quad \max_{\boldsymbol{V}, t} \ t \tag{37a}$$

Algorithm 1: Gaussian Randomization Procedure for Obtaining Rank-One Solution.

Input: The solution: $\boldsymbol{V}^\star$, a large positive integer I, and an empty set $\mathbb{G}$.

Output: Optimal phase shifts: $\boldsymbol{\theta}^{(l)}$.

1:    Conduct *singular value decomposition* (SVD) of $\boldsymbol{V}^\star$ as $\boldsymbol{V}^\star = \boldsymbol{U}_v \boldsymbol{\Sigma}_v \boldsymbol{U}_v^H$, with $\boldsymbol{U}_v = [\boldsymbol{u}_{v,1}, \dots, \boldsymbol{u}_{v,N+1}]$.

2:    **for** $i = 1$ to I **do**

3:      Generate a vector $\boldsymbol{v}_i = \boldsymbol{U}_v \boldsymbol{\Sigma}_v^{\frac{1}{2}} \boldsymbol{e}_i$, where $\boldsymbol{e}_i \sim \mathcal{CN}(\boldsymbol{0}_{N+1}, \boldsymbol{I}_{N+1})$.

4:      **if** P1-B4 is feasible with $\boldsymbol{v}_i$, **then**

5:        Obtain $\boldsymbol{\theta}_i = [\arg(\frac{\boldsymbol{v}_i}{[\boldsymbol{v}_i]_{end}})]_{1:N}$, $\mathbb{G} = \mathbb{G} \cup \boldsymbol{\theta}_i$, compute $\widehat{\gamma}(\boldsymbol{\theta}_i) = |\boldsymbol{g}^H \boldsymbol{\Theta}_i \boldsymbol{H} \boldsymbol{w}|^2$,

6:      **end if**

7:    **end for**

8:    Obtain the rank-one solution $\boldsymbol{\theta}^\star = \arg\max_{\boldsymbol{\theta}_i \in \mathbb{G}} \ \widehat{\gamma}(\boldsymbol{\theta}_i)$

9:    **return** $\theta_{n,1-bit}^\star = \arg\min_{\theta \in \{0, \pi\}} |\theta - \theta_n^\star|, n = 1, \dots, N.$

$$\text{s.t.} \ \frac{\gamma_s(\boldsymbol{V})}{\Gamma_s} \geq t, \tag{37b}$$

$$\frac{\gamma_c(\boldsymbol{V})}{\Gamma_c} \geq t, \tag{37c}$$

$$t \geq 1, \tag{37d}$$

$$(36c), (36d). \tag{37e}$$

The SDR technique can be applied to solve P1-B4. When we obtain the solution $\boldsymbol{V}^{(l)}$, then substitute it into the active beamforming related problem P1-A1 to obtain $\boldsymbol{w}^{(l+1)}$. By doing so, the subproblem P1-A1 and P1-B4 are solved iteratively until convergence. Finally, the converged solution $\boldsymbol{V}^\star$ may not be rank-one due to the relaxation. Hence, the Gaussian randomization procedure is used to obtain a rank-one solution [14]. The main idea is to generate a set of candidate vectors $\{\boldsymbol{v}_i\}$ using $\boldsymbol{V}^\star$, then select the best one from the set. The details are given in Algorithm 1.

2) Phase Shifter With Any-Bit Resolutions: As for the high-resolution phase shifter, if we sill use the SDR technique, it will incur high computational complexity when N is large. With the increasing of the number of quantization bits (i.e., b), its discrete phase shift set given by $\mathcal{A}_2 \triangleq \{\theta | \theta \in \{0, \frac{2\pi}{2^b}, \dots, \frac{2\pi}{2^b}(2^b - 1)\}\}$ will be closer to the continuous set $\mathcal{A}_1 \triangleq \{\theta | \theta \in [0, 2\pi)\}$. Therefore, we can directly quantifying the continuous phase shifts to its nearest point in the discrete set without sacrificing severe performance loss as compared to the SDR technique. Specifically, we first relax the discrete constraint by considering its continuous counterparts, and then directly quantize the continuous phase shifts given in Theorem 1 to its nearest discrete feasible point, given by

$$\theta_{n,\text{Any-bit}}^\star = \arg\min_{\theta \in \mathcal{A}_2} |\theta - \theta_n^\star|, n = 1, \dots, N, \tag{38}$$

where $\boldsymbol{\theta}^\star$ is the optimal solution to continuous phase shifter.

TABLE I
COMPLEXITY ANALYSIS FOR THE PROPOSED ALGORITHMS

CSI	Active Beamforming-associated Subproblem	Passive Beamforming-associated Subproblem
Perfect CSI	$\mathcal{O}(2^{3.5}\log(1/\varsigma))$	Continuous Phase Shifter: $\mathcal{O}(1)$ due to the closed-form solution
		1-bit Phase Shifter: $\mathcal{O}((N+1)^{3.5}\log(1/\varsigma))$
		Any-bit Phase Shifter: $\mathcal{O}(2^b N)$
Imperfect CSI	$\mathcal{O}(\log(1/\varsigma)[2(2M(N+1))+1]^{1/2}M[M^2 + 2M(2M(N+1)+1)^2 + 2(2M(N+1)+1)^3])$	Continuous Phase Shifter &1-bit Phase Shifter: $\mathcal{O}(\log(1/\varsigma)[2(2M(N+1))+1]^{1/2}(N+1)[(N+1)^2 + 2(N+1)(2M(N+1)+1)^2 + 2(2M(N+1)+1)^3])$
		Any-bit Phase Shifter: $\mathcal{O}(\log(1/\varsigma)[2(2M(N+1))+1]^{1/2}(N+1)[(N+1)^2 + 2(N+1)(2M(N+1)+1)^2 + 2(2M(N+1)+1)^3] + 2^b N)$

D. Convergence and Complexity Analysis

1) Convergence: The overall procedure for solving problem P1 is shown in Algorithm 2. The algorithm is initialized with $\boldsymbol{w}^{(0)}$ and $\boldsymbol{V}^{(0)}$ chosen from feasible sets, and then $\boldsymbol{w}^{(l)}$ and $\boldsymbol{V}^{(l)}$ are optimized alternatively in the l-th iteration. The proposed algorithm is guaranteed to converge since the transmit power p is monotonically non-increasing over the iterations, i.e., $p(\boldsymbol{w}^{(l-1)};\boldsymbol{V}^{(l-1)}) \overset{a}{\geq} \min_{\boldsymbol{w}} p(\boldsymbol{w};\boldsymbol{V}^{(l)}) = p(\boldsymbol{w}^{(l)};\boldsymbol{V}^{(l-1)}) \overset{b}{=} p(\boldsymbol{w}^{(l)};\boldsymbol{V}^{(l)})$, where "$a$" is true since P1-A2 is a convex problem, and "b" holds since P1-B4 is a feasibility checking problem. Hence, we have proved that $p(\boldsymbol{w}^{(l-1)};\boldsymbol{V}^{(l-1)}) \geq p(\boldsymbol{w}^{(l)};\boldsymbol{V}^{(l)})$, which can guarantee to converge to a local (global) optimal solution.

2) Complexity Analysis: According to [43], [44], by utilizing the interior-point method algorithm, it can be shown that the computational complexity for solving the SDP problem P1-A1 is $\mathcal{O}(2^{3.5}\log(1/\varsigma))$, where ς accounts for the precision of the interior point algorithm. For the problem P1-B1, we omit the complexity of obtaining the closed-form solution given in Theorem 1; for the one-bit phase shifter, the complexity for solving P1-B4 is $\mathcal{O}((N+1)^{3.5}\log(1/\varsigma))$; while for the any-bit phase shifter, the complexity of the quantization method is $\mathcal{O}(2^b N)$. Denote by I_O the iteration number of the AO algorithm, then the overall complexity of Algorithm 2 with one-bit phase shifter is $\mathcal{O}(I_O(2^{3.5}\log(1/\varsigma) + (N+1)^{3.5}\log(1/\varsigma)))$, while for the continuous and any-bit phase shifter, the complexity of Algorithm 2 are $\mathcal{O}(I_O(2^{3.5}\log(1/\varsigma)))$ and $\mathcal{O}(I_O(2^{3.5}\log(1/\varsigma)) + 2^b N)$, respectively. The details of the complexity analysis are summarized in Table I.

IV. COOPERATIVE BEAMFORMING DESIGN FOR THE IMPERFECT CSI CASE

In the previous section, cooperative beamforming design is investigated under the perfect CSI setup. Nevertheless, in practice, it is challenging to obtain perfect CSI, which motivates us in this section to study robust beamforming for the RIS-assisted SR system.

Recall that variables $\boldsymbol{H}_1$, $\boldsymbol{H}_2$, $\boldsymbol{H}_3$, $\boldsymbol{H}_4$ and $\boldsymbol{v}$ defined in the Section II, under the imperfect CSI setup, they can be rewritten as

$$\boldsymbol{H}_k = \widetilde{\boldsymbol{H}}_k + \Delta \boldsymbol{H}_k, k = 1,\dots,4, \tag{39}$$

Algorithm 2: AO Algorithm for P1 with Perfect CSI.

1: Initialize $\boldsymbol{w}^{(0)}, \boldsymbol{\theta}^{(0)}, \boldsymbol{V}^{(0)}$ and iteration number $l = 0$.
2: **repeat**
3:     Obtain $\boldsymbol{w}^{(l+1)}$ by solving the problem P1-A1 with given $\boldsymbol{V}^{(l)}$.
4:     Obtain $\boldsymbol{V}^{(l+1)}$ with given $\boldsymbol{w}^{(l+1)}$, in terms of different phase shifters (i.e., continuous, 1-bit, any-bit).
5:     Update $l \leftarrow l + 1$.
6: **until** the transmit power, i.e., $\text{tr}(||\boldsymbol{w}^{(l)}||^2)$ converges.
7: Obtain optimal solutions $\boldsymbol{w}^{\star}$ and $\boldsymbol{\theta}^{\star}$ according to different phase shifters.

---

where $\widetilde{\boldsymbol{H}}_1 = \begin{bmatrix} \widetilde{\boldsymbol{G}} \\ \widetilde{\boldsymbol{h}}^H \end{bmatrix}$, $\widetilde{\boldsymbol{H}}_2 = \begin{bmatrix} -\widetilde{\boldsymbol{G}} \\ \widetilde{\boldsymbol{h}}^H \end{bmatrix}$, $\widetilde{\boldsymbol{H}}_3 = \begin{bmatrix} \widetilde{\boldsymbol{G}} \\ \boldsymbol{0}_M \end{bmatrix}$, and $\widetilde{\boldsymbol{H}}_4 = \begin{bmatrix} \boldsymbol{0}_{N\times M} \\ \widetilde{\boldsymbol{h}}^H \end{bmatrix}$ denote the estimated composite channels, $\Delta \boldsymbol{H}_1 = \begin{bmatrix} \Delta \boldsymbol{G} \\ \Delta \boldsymbol{h}^H \end{bmatrix}$, $\Delta \boldsymbol{H}_2 = \begin{bmatrix} -\Delta \boldsymbol{G} \\ \Delta \boldsymbol{h}^H \end{bmatrix}$, $\Delta \boldsymbol{H}_3 = \begin{bmatrix} \Delta \boldsymbol{G} \\ \boldsymbol{0}^H \end{bmatrix}$, and $\Delta \boldsymbol{H}_4 = \begin{bmatrix} \boldsymbol{0}_{N\times M} \\ \Delta \boldsymbol{h}^H \end{bmatrix}$ represent the composite CSI errors.

In addition to variable $\boldsymbol{V}$ defined in Section III-A, we introduce another variable $\boldsymbol{W}$, which satisfies $\boldsymbol{W} \succeq 0$, $\text{rank}(\boldsymbol{W}) = 1$. By using SDR technique to relax the rank-one constraints of $\boldsymbol{W}$ and $\boldsymbol{V}$, the problem P2 can be recast as

$$\underline{P2'}: \quad \min_{\boldsymbol{W},\boldsymbol{V}} \text{tr}(\boldsymbol{W}) \tag{40a}$$

$$\text{s.t.} \, \text{tr}(\boldsymbol{V}\boldsymbol{H}_1\boldsymbol{W}\boldsymbol{H}_1^H) + \text{tr}(\boldsymbol{V}\boldsymbol{H}_2\boldsymbol{W}\boldsymbol{H}_2^H) \geq 2\Gamma_s\sigma^2, \tag{40b}$$

$$\frac{\text{tr}(\boldsymbol{V}\boldsymbol{H}_3\boldsymbol{W}\boldsymbol{H}_3^H)}{\delta\text{tr}(\boldsymbol{V}\boldsymbol{H}_4\boldsymbol{W}\boldsymbol{H}_4^H) + \frac{\sigma^2}{K}} \geq \Gamma_c \tag{40c}$$

$$[\boldsymbol{V}]_{n,n} = 1, \forall n = 1,\dots,N+1, \tag{40d}$$

$$\Delta \boldsymbol{H}_1 \in \mathcal{H}_1, \Delta \boldsymbol{H}_2 \in \mathcal{H}_2, \Delta \boldsymbol{H}_3 \in \mathcal{H}_3, \Delta \boldsymbol{H}_4 \in \mathcal{H}_4 \tag{40e}$$

$$\boldsymbol{W} \succeq 0, \tag{40f}$$

$$\boldsymbol{V} \succeq 0, \tag{40g}$$

where $\mathcal{H}_1, \mathcal{H}_2, \mathcal{H}_3, \mathcal{H}_4$ denote the CSI error sets of the composite channels $\boldsymbol{H}_1, \boldsymbol{H}_2, \boldsymbol{H}_3$ and $\boldsymbol{H}_4$, respectively.

A. AO Algorithm for P2′

P2′ is a non-convex problem due to its non-convex constraints. Moreover, the imperfect SIC and the bounded CSI error constraints make the problem more challenging. Fortunately, the AO algorithm can still be utilized to split P2′ into two subproblems, which are solved iteratively until the convergence. The two decomposed subproblems are expressed as

$$\underline{\textbf{P2-A}}: \quad \min_{\boldsymbol{W}} \operatorname{tr}(\boldsymbol{W}) \tag{41a}$$

$$\text{s.t. } (40b), (40c), (40e), (40f), \tag{41b}$$

and

$$\underline{\textbf{P2-B}}: \quad \min_{\boldsymbol{V}} \operatorname{tr}(\boldsymbol{W}) \tag{42a}$$

$$\text{s.t. } (40b), (40c), (40d), (40e), (40g). \tag{42b}$$

The challenge to solve P2-A and P2-B lies in the semi-infinite constraints caused by the channel uncertainty (40e). To address this, we transform them into deterministic constraints by employing a tool called S-Lemma, please refer to [21, Lemma 1] for more details of S-Lemma.

We first rewrite the constraints (40b) and (40c) using (39). The constraint of primary transmission (40b) becomes

$$\operatorname{tr}(\boldsymbol{V}\boldsymbol{H}_1\boldsymbol{W}\boldsymbol{H}_1^H) + \operatorname{tr}(\boldsymbol{V}\boldsymbol{H}_2\boldsymbol{W}\boldsymbol{H}_2^H) \geq 2\Gamma_s\sigma^2 \tag{43}$$

$$\overset{a}{\Leftrightarrow} \operatorname{vec}^H\left(\widetilde{\boldsymbol{H}}_1 + \Delta\boldsymbol{H}_1\right)(\boldsymbol{W}\otimes\boldsymbol{V})\operatorname{vec}\left(\widetilde{\boldsymbol{H}}_1 + \Delta\boldsymbol{H}_1\right)$$

$$+\operatorname{vec}^H\left(\widetilde{\boldsymbol{H}}_2 + \Delta\boldsymbol{H}_2\right)(\boldsymbol{W}\otimes\boldsymbol{V})\operatorname{vec}\left(\widetilde{\boldsymbol{H}}_2 + \Delta\boldsymbol{H}_2\right) \geq 2\Gamma_s\sigma^2 \tag{44}$$

$$\overset{b}{\Leftrightarrow} \left[\boldsymbol{\alpha}^H\boldsymbol{U}\boldsymbol{\alpha} + 2\Re\left\{\boldsymbol{\alpha}^H\boldsymbol{U}\boldsymbol{\beta}\right\} + \boldsymbol{\beta}^H\boldsymbol{U}\boldsymbol{\beta}\right] \geq 2\Gamma_s\sigma^2, \tag{45}$$

where "a" holds due to the matrix equality, i.e., $\operatorname{tr}(\boldsymbol{A}^H\boldsymbol{B}) = \operatorname{vec}^H(\boldsymbol{A})\operatorname{vec}(\boldsymbol{B})$ and $\operatorname{vec}(\boldsymbol{ABC}) = (\boldsymbol{C}^H\otimes\boldsymbol{A})\operatorname{vec}(\boldsymbol{B})$, "$b$" follows from the following definitions

$$\boldsymbol{\alpha} = \left[\operatorname{vec}^H\left(\Delta\boldsymbol{H}_1\right), \operatorname{vec}^H\left(\Delta\boldsymbol{H}_2\right)\right]^H \in \mathbb{C}^{2M(N+1)}, \tag{46}$$

$$\boldsymbol{\beta} = \left[\operatorname{vec}^H\left(\widetilde{\boldsymbol{H}}_1\right), \operatorname{vec}^H\left(\widetilde{\boldsymbol{H}}_2\right)\right]^H \in \mathbb{C}^{2M(N+1)}, \tag{47}$$

$$\boldsymbol{U} = \operatorname{blkdiag}\left(\boldsymbol{W}\otimes\boldsymbol{V}, \boldsymbol{W}\otimes\boldsymbol{V}\right) \in \mathbb{C}^{2M(N+1)\times 2M(N+1)}. \tag{48}$$

According to [21], the channel uncertainty constraints, i.e., (40e), can be equivalently expressed in the following quadratic forms

$$\boldsymbol{\alpha}^H\boldsymbol{A}_i\boldsymbol{\alpha} - \varepsilon_g^2 \leq 0, \forall i = 1, 3. \boldsymbol{\alpha}^H\boldsymbol{A}_i\boldsymbol{\alpha} - \varepsilon_h^2 \leq 0, \forall i = 2, 4. \tag{49}$$

where

$$\boldsymbol{A}_1 = \operatorname{diag}(\underbrace{\boldsymbol{b}, \ldots, \boldsymbol{b}}_{M}, \boldsymbol{0}_{(N+1)M}), \boldsymbol{A}_2 = \operatorname{diag}(\underbrace{\boldsymbol{c}, \ldots, \boldsymbol{c}}_{M}, \boldsymbol{0}_{(N+1)M}),$$

$$\boldsymbol{A}_3 = \operatorname{diag}(\boldsymbol{0}_{(N+1)M}, \underbrace{\boldsymbol{b}, \ldots, \boldsymbol{b}}_{M}), \boldsymbol{A}_4 = \operatorname{diag}(\boldsymbol{0}_{(N+1)M}, \underbrace{\boldsymbol{c}, \ldots, \boldsymbol{c}}_{M}),$$

$$\boldsymbol{b} = [\boldsymbol{1}_N, 0] \in \mathbb{C}^{N+1}, \boldsymbol{c} = [0, \boldsymbol{1}_N] \in \mathbb{C}^{N+1}.$$

Then, according to the general S-Lemma, by introducing an auxiliary vector $\boldsymbol{t} = [t_1, t_2, t_3, t_4]^T \geq 0$, the equivalent constraints (45) and (49) can be equivalently transformed into the following linear matrix inequality.

$$\begin{bmatrix} \boldsymbol{U} + \sum_{i=1}^4 t_i\boldsymbol{A}_i & \boldsymbol{U}\boldsymbol{\beta} \\ (\boldsymbol{U}\boldsymbol{\beta})^H & C_1 \end{bmatrix} \succeq 0, \tag{51}$$

where $C_1 = \boldsymbol{\beta}^H\boldsymbol{U}\boldsymbol{\beta} - 2\sigma^2\Gamma_s - (t_1 + t_3)\varepsilon_g^2 - (t_2 + t_4)\varepsilon_h^2$.

Similarly, we can rewritten the constraint (40c) as follows

$$\boldsymbol{\eta}^H\boldsymbol{T}\boldsymbol{\eta} + 2\Re\left\{\boldsymbol{\eta}^H\boldsymbol{T}\boldsymbol{r}\right\} + \boldsymbol{r}^H\boldsymbol{T}\boldsymbol{r} - \frac{1}{K}\sigma^2\Gamma_c \geq 0, \tag{52}$$

where

$$\boldsymbol{\eta} = \left[\operatorname{vec}^H\left(\Delta\boldsymbol{H}_3\right), \operatorname{vec}^H\left(\Delta\boldsymbol{H}_4\right)\right]^H \in \mathbb{C}^{2M(N+1)}, \tag{53}$$

$$\boldsymbol{r} = \left[\operatorname{vec}^H\left(\widetilde{\boldsymbol{H}}_3\right), \operatorname{vec}^H\left(\widetilde{\boldsymbol{H}}_4\right)\right]^H \in \mathbb{C}^{2M(N+1)}, \tag{54}$$

$$\boldsymbol{T} = \operatorname{blkdiag}\left(\boldsymbol{W}\otimes\boldsymbol{V}, -\Gamma_c\delta\left(\boldsymbol{W}\otimes\boldsymbol{V}\right)\right)$$

$$\in \mathbb{C}^{2M(N+1)\times 2M(N+1)}. \tag{55}$$

And the channel uncertainties, i.e., (40e), can be expressed in terms of $\boldsymbol{\eta}$ [21]

$$\boldsymbol{\eta}^H\boldsymbol{A}_1\boldsymbol{\eta} - \varepsilon_g^2 \leq 0, \boldsymbol{\eta}^H\boldsymbol{A}_2\boldsymbol{\eta} \leq 0, \tag{56}$$

$$\boldsymbol{\eta}^H\boldsymbol{A}_4\boldsymbol{\eta} - \varepsilon_h^2 \leq 0, \boldsymbol{\eta}^H\boldsymbol{A}_3\boldsymbol{\eta} \leq 0. \tag{57}$$

By using the S-Lemma, the constraints (52), (56) and (57) are valid if and only if there exists a vector $\boldsymbol{q} = [q_1, q_2, q_3, q_4]^T \geq 0$ such that the following inequality is valid.

$$\begin{bmatrix} \boldsymbol{T} + \sum_{i=1}^4 q_i\boldsymbol{A}_i & \boldsymbol{T}\boldsymbol{r} \\ (\boldsymbol{T}\boldsymbol{r})^H & C_2 \end{bmatrix} \succeq 0, \tag{58}$$

where $C_2 = \boldsymbol{r}^H\boldsymbol{T}\boldsymbol{r} - \frac{1}{K}\sigma^2\Gamma_c - q_1\varepsilon_g^2 - q_4\varepsilon_h^2$.

Then, the semi-infinite constraints are transformed into equivalent finite constraints, i.e., (51), (58). Further, P2-A and P2-B can be transformed into convex SDP problems.

$$\underline{\textbf{P2-A1}}: \quad \min_{\boldsymbol{W}, \{t_i\}_{i=1}^4 \geq 0, \{q_i\}_{i=1}^4 \geq 0} \operatorname{tr}(\boldsymbol{W}) \tag{59a}$$

$$\text{s.t. } (51), (58), (40f), \tag{59b}$$

and

$$\underline{\textbf{P2-B1}}: \quad \min_{\boldsymbol{V}, \{x_i\}_{i=1}^4 \geq 0, \{y_i\}_{i=1}^4 \geq 0} \operatorname{tr}(\boldsymbol{W}) \tag{60a}$$

$$\text{s.t. } (51), (58), (40d), (40g) \tag{60b}$$

Note that the P2-A1 is now a standard convex SDP problem, which can be efficiently solved by existing optimization tools, i.e., CVX. However, P2-B1 is a feasibility checking problem. To obtain a feasible solution which guarantees the convergence of the whole AO algorithm, according to [22], we consider P2-B1 with the modified constraint (40d), i.e., $[\widetilde{\boldsymbol{V}}]_{n,n} = e$, $n = 1, \ldots, N+1$, and $0 < e \leq 1$. If the solution $(\widetilde{\boldsymbol{V}}, \boldsymbol{W})$ satisfies the rest of constraints in P2-B1, then the solution $(\frac{1}{e}\widetilde{\boldsymbol{V}}, e\boldsymbol{W})$ can guarantee all the original constraints in P2-B1 while achieving a lower power, i.e., $\operatorname{tr}(e\boldsymbol{W})$. Thus, we introduce an auxiliary

---

Algorithm 3: AO Algorithm for P2 with Imperfect CSI.

1: Initialize $\boldsymbol{W}^{(0)} = \boldsymbol{w}\boldsymbol{w}^H$ and $\boldsymbol{V}^{(0)} = \boldsymbol{v}\boldsymbol{v}^H$, and iteration number $l = 0$.
2: **repeat**
3: Obtain optimal $\boldsymbol{W}^{(l+1)}$ by solving the problem P2-A1 with given $\boldsymbol{V}^{(l)}$.
4: Obtain optimal $\widetilde{\boldsymbol{V}}^{(l+1)}$ and $e^{(l+1)}$ by solving problem P2-B2 with given $\boldsymbol{W}^{(l+1)}$.
5: $\boldsymbol{W}^{(l+1)} \leftarrow e^{(l+1)}\boldsymbol{W}^{(l+1)}$, $\boldsymbol{V}^{(l+1)} \leftarrow \frac{1}{e^{(l+1)}}\widetilde{\boldsymbol{V}}^{(l+1)}$.
6: Update $l \leftarrow l + 1$.
7: **until** the transmit power, i.e., $\text{tr}(\boldsymbol{W}^{(l)})$ converges.
8: Obtain $\boldsymbol{w}^\star$ and $\boldsymbol{\theta}^\star$ via Gaussian randomization with given $\boldsymbol{W}^{(l)}$ and $\boldsymbol{V}^{(l)}$, in terms of different phase shifter(i.e., continuous, 1-bit, any-bit).

---

variable e, and transform P2-B1 into the following problem, i.e., P2-B2. By solving P2-B2, the convergence of the AO algorithm can be guaranteed.

$$
\textbf{P2-B2}: \min_{\widetilde{\boldsymbol{V}}, \{x_i\}_{i=1}^4 \geq 0, \{y_i\}_{i=1}^4 \geq 0, e} e \tag{61a}
$$

$$
\text{s.t.} \quad (51), (58), (40d), (40g), \tag{61b}
$$

$$
[\widetilde{\boldsymbol{V}}]_{n,n} = e, \forall n = 1, \ldots, N+1, \tag{61c}
$$

$$
0 < e \leq 1. \tag{61d}
$$

Similarly, P2-B2 is a standard convex SDP, which can be tackled by CVX, and then the final solution can be calculated as $\boldsymbol{V}^{(l)} \leftarrow \frac{1}{e}\widetilde{\boldsymbol{V}}^{(l)}$. Therefore, using the AO algorithm, the two subproblems P2-A1 and P2-B2 are solved iteratively.

After we obtain the converged solutions $\boldsymbol{W}^\star$ and $\boldsymbol{V}^\star$, Gaussian randomization method is used to obtain final solution $\boldsymbol{w}^\star$ and $\boldsymbol{\theta}^\star$. Specifically, To be specific, we first decompose $\boldsymbol{W}^\star$ and $\boldsymbol{V}^\star$ as $\boldsymbol{W}^\star = \boldsymbol{U_w}\boldsymbol{\Sigma_w}\boldsymbol{U_w}^H$, $\boldsymbol{V}^\star = \boldsymbol{U_v}\boldsymbol{\Sigma_v}\boldsymbol{U_v}^H$, where $\boldsymbol{U_w}$ and $\boldsymbol{U_v}$ are the unitary matrices, $\boldsymbol{\Sigma_w}$ and $\boldsymbol{\Sigma_v}$ are the diagonal matrix whose diagonal elements are the singular value of $\boldsymbol{W}^\star$ and $\boldsymbol{V}^\star$, respectively. Then, we generate D random vectors, e.g., $\boldsymbol{w}_d = \boldsymbol{U_w}\boldsymbol{\Sigma_w}^{\frac{1}{2}}\boldsymbol{e}_d$, $\boldsymbol{v}_d = \boldsymbol{U_v}\boldsymbol{\Sigma_v}^{\frac{1}{2}}\boldsymbol{e}_d$, $\boldsymbol{\theta}_d = [\arg(\frac{\boldsymbol{v}_d}{[\boldsymbol{v}_d]_{\text{end}}})]_{1:N}$, where $\boldsymbol{e}_d \sim \mathcal{CN}(0, \boldsymbol{I}_M)$ with $\boldsymbol{I}_M \in \mathbb{R}^{M \times M}$ denoting an identity matrix, then we incorporate them into a set $\mathbb{Q}$ and $\mathbb{F}$. Finally, we take the value of $\boldsymbol{w}^\star = \arg\min_{\boldsymbol{w}\in\mathbb{Q}} \|\boldsymbol{w}\|_2^2$, $\boldsymbol{\theta}^\star = \arg\max_{\boldsymbol{\theta}\in\mathbb{F}} |\boldsymbol{g}^H\boldsymbol{\Theta}\boldsymbol{H}\boldsymbol{w}^\star|^2$.

Remark 3: We can obtain the continuous phase shifts using the above Gaussian randomization method. As for 1-bit phase shifter design, we can use the Algorithm 1 with input $\boldsymbol{V}^\star$ to obtain 1-bit phase shifts. For the any-bit phase shifter, we directly quantize the obtained continuous phase shifts into the discrete space.

B. Convergence and Complexity Analysis

1) Convergence: The detailed process for solving P2′ is summarized in Algorithm 3, $\boldsymbol{W}^{(l)}$ and $\boldsymbol{V}^{(l)}$ are iteratively updated over the iterations. Then the optimal $\boldsymbol{w}^\star$ and $\boldsymbol{\theta}^\star$ are obtained

from the converged $\boldsymbol{W}^{(l)}$ and $\boldsymbol{V}^{(l)}$. Algorithm 3 can guarantee the convergence of P2′, proof is omitted here due to the similarity with Section III-D.

2) Complexity Analysis: According to [21], [43], the problem **P2-A1** and **P2-B2** can be solved by the standard interior point method, and the general expression of the complexity is given by

$$
\mathcal{O}\left(\left(\sum_{j=1}^J b_j + 2I\right)^{1/2} k\left(k^2 + k\sum_{j=1}^J b_j^2 + \sum_{j=1}^J b_j^3 + k\sum_{i=1}^I m_i^2\right)\right), \tag{62}
$$

where k denotes the number of variables, J denotes the number of *linear matrix inequalitys* (LMIs) with size b_j, I denotes the number of second-order cone constraints with size m_i. Based on this expression, we summarize and provide the complexity analysis for solving these problems in Table I.

V. SIMULATION RESULTS

In this section, numerical results are presented to demonstrate the performance of the proposed algorithms. Following the parameter settings in other works [14], [26], we set the PTx-RIS link distance $d_1 = 200$ (m), the PTx-PRx link distance $d_2 = 202$ (m), the RIS-PRx link distance[6] $d_3 = 3$ (m). The Rician factors are set as $\kappa_1 = 10$ dB, $\kappa_2 = 3$ dB, $\kappa_3 = 3$ dB. The path loss exponent as $\alpha_1 = 2$, $\alpha_2 = 3.5$, $\alpha_3 = 2.8$. The AoD of PTx-PRx and PTx-RIS links are set as $\varphi_{TR}^D = -0.4\pi$, $\varphi_{TL}^D = 0.6\pi$, the azimuth and elevation AoA of PTx-RIS link are set as $\vartheta_{TL}^A = 0.8\pi$ and $\phi_{TL}^A = 0.05\pi$, the azimuth and elevation AoD of RIS-PRx link are set as $\vartheta_{LR}^D = -0.5\pi$ and $\phi_{LR}^D = 0.1\pi$. We set $\beta_0 = -40$ dB according to the 3GPP UMi model [45] with carrier frequency 3.5 GHz, the number of PTx antennas $M = 4$, and the noise power $\sigma^2 = -100$ dBm. In addition, we set $\Gamma_s = 20$ dB, $\Gamma_c = 5$ dB, spreading gain $K = 100$.

A. Perfect CSI Case

For the perfect CSI case, in order to reveal the insights of RIS-assisted SR system, we compare the proposed algorithms with the following baselines that are commonly used in the existing literature [14], [15].

- *Baseline 1 (Without RIS):* i.e., $N = 0$, the formulated problem degrades to the conventional transmit power minimization problem;
- *Baseline 2 (Random phase shifts):* phase shifts are uniformly chosen from continuous feasible sets;
- *Baseline 3 (PTx-PRx MRT):* We set the normalized PTx transmit beamforming vector as $\overline{\boldsymbol{w}} = \frac{\boldsymbol{h}}{\|\boldsymbol{h}\|_2}$ based on the PTx-PRx channel. Denote p as the transmit power at the PTx, we have the transmit beamforming vector $\boldsymbol{w} = \sqrt{p}\overline{\boldsymbol{w}}$. The phase shifts $\boldsymbol{\theta}^\star$ are obtained using Theorem 1. Finally,

---

[6]To reap more passive beamforming gain brought by the RIS, the RIS is deployed close to the PRx.
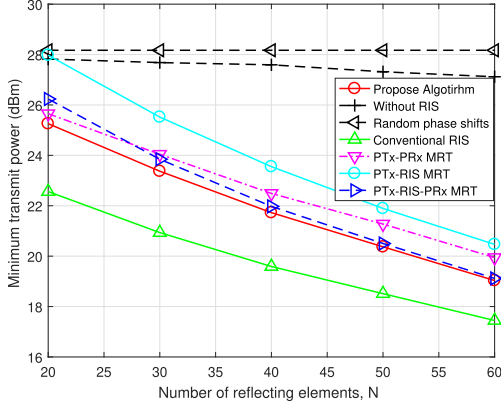
Fig. 3.   Power versus number of reflecting elements N: Primary transmission requirement $\Gamma_s = 20$ dB, RIS transmission requirement $\Gamma_c = 5$ dB, spreading gain $K = 100$.
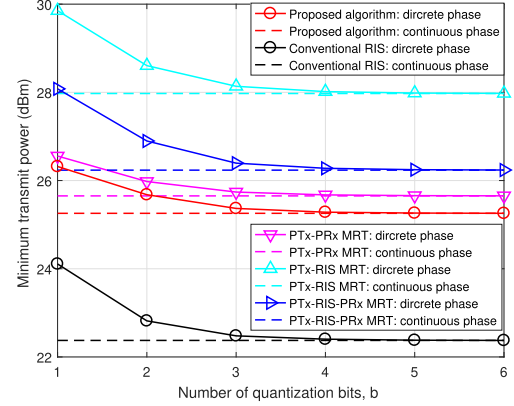

Fig. 4.   Power versus number of quantization bits b: Primary transmission requirement $\Gamma_s = 20$ dB, RIS transmission requirement $\Gamma_c = 5$ dB, number of reflecting elements $N = 20$, spreading gain $K = 100$.

the transmit power is calculated as

$$p = \max\left(P_{\mathrm{s,min}}, P_{\mathrm{c,min}}\right). \qquad (63)$$

where $P_{\mathrm{s,min}} = \frac{2\sigma^2\Gamma_s}{|(\boldsymbol{h}^H + \boldsymbol{g}^H\boldsymbol{\Theta}^\star\boldsymbol{H})\overline{\boldsymbol{w}}|^2 + |(\boldsymbol{h}^H - \boldsymbol{g}^H\boldsymbol{\Theta}^\star\boldsymbol{H})\overline{\boldsymbol{w}}|^2}$,
$P_{\mathrm{c,min}} = \frac{\sigma^2\Gamma_c}{K|\boldsymbol{g}^H\boldsymbol{\Theta}^\star\boldsymbol{H}\overline{\boldsymbol{w}}|^2}$.

- *Baseline 4 (PTx-RIS MRT):* We set the normalized PTx transmit beamforming vector as $\overline{\boldsymbol{w}} = \frac{\boldsymbol{h}_0}{\|\boldsymbol{h}_0\|_2}$ based on the PTx-RIS rank-one channel, where $\boldsymbol{h}_0$ is any row in the channel $\boldsymbol{H}$. Similarly, the transmit beamforming vector $\boldsymbol{w} = \sqrt{p}\overline{\boldsymbol{w}}$. The optimal phase shifts $\boldsymbol{\theta}^\star$ are obtained via Theorem 1. The minimum transmit power p is given by (63).

- *Baseline 5 (PTx-RIS-PRx MRT):* In the alternating optimization algorithm, when solving the subproblem P1-A, we set the normalized transmit beamforming vector as $\overline{\boldsymbol{w}} = \frac{\boldsymbol{f}}{\|\boldsymbol{f}\|_2}$, where $\boldsymbol{f} \triangleq (\boldsymbol{g}^H\boldsymbol{\Theta}\boldsymbol{H})^H$, when solving the subproblem P1-B, the optimal phase shifts $\boldsymbol{\theta}^\star$ is given in the Theorem 1, and then the transmit power is given by (63). Then, we iteratively solve P1-A and P1-B until convergence.

- *Baseline 6 (Conventional RIS):* RIS does not transmit its information, it is only used to enhance backscatter link. The algorithm proposed in [14] is utilized to solve the RIS-aided power minimization problem.

Fig. 3 shows the transmit power with respect to the number of reflecting elements under different schemes. First, it is observed that the power decreases with the increasing of the N at the RIS. The reason is as follows. The more reflecting elements, the stronger the backscatter link. Thus, PTx needs less power to fulfill its signal transmission under the same SNR constraints. Second, it can be seen that PTx-PRx MRT and PTx-RIS-PRx MRT baselines perform closely to the proposed algorithm. Obviously, the two baselines can be viewed as special cases of the proposed algorithm by setting the normalized transmit beamforming vector as $\overline{\boldsymbol{w}} = \frac{\boldsymbol{h}}{\|\boldsymbol{h}\|_2}$ and $\overline{\boldsymbol{w}} = \frac{\boldsymbol{f}}{\|\boldsymbol{f}\|_2}$. Interestingly, we find that for small N, PTx-PRx MRT outperforms the PTx-RIS-PRx MRT. However, when N exceeds 30, PTx-RIS-PRx MRT is better than PTx-PRx MRT. This is because when N is small, the backscatter link is much weaker than the direct link,

the PTx would like to beam towards the direct link to fulfill transmission. When N goes larger, the backscatter link is much stronger, then PTx would choose to beam towards the backscatter link to satisfy the SNR requirement. This observation verifies our analysis in Remark 2.

On the other hand, we can see that for Baseline 6 (Conventional RIS) in Fig. 3, it needs less transmit power than the proposed algorithm. The reason is as follows, conventional RIS is used purely to aid the wireless links, once the phase shifts matrix is optimized, it is fixed. While for the RIS-assisted symbiotic radio system, RIS has two functions, namely, assisting the wireless links and transmitting its information. For this type of use, RIS will change its phase shifts periodically according to its transmitted symbols. Therefore, compared with the conventional RIS, more power is needed to transmit the additional RIS information.

Fig. 4 plots the transmit power versus the number of quantization bits under different schemes. The results under continuous phase shifts design serve as a lower bound, one can see that more power is required in discrete phase shifts scenario. As the number of quantization bits b increases, the gap between continuous and discrete phase shifts becomes negligible. This is because with the increasing of b, its discrete phase shift set given by $\mathcal{A}_2 \triangleq \{\theta | \theta \in \{0, \frac{2\pi}{2^b}, \ldots, \frac{2\pi}{2^b}(2^b - 1)\}\}$ will be closer to the continuous set $\mathcal{A}_1 \triangleq \{\theta | \theta \in [0, 2\pi)\}$. For the proposed algorithm, the transmit power increases by 4.2%, 1.7%, 0.4% as compared to continuous phase shifts design, when $b = 1, 2, 3$, respectively. Particularly, the performance of the 3-bit phase shifter is capable of approaching that of a continuous counterpart.

In Fig. 5, we investigate the how the SNR requirements of primary and RIS transmissions affect the system performance with $N = 20$. One can observe that for fixed Γ_s, the transmit power first remains unchanged, then it gradually increases as Γ_c goes larger. Interestingly, when Γ_c is greater than 15 dB, the RIS-assisted symbiotic radio system shows almost the same power for $\Gamma_s = -10$ dB, -5 dB, -3 dB, respectively. In the low Γ_c regime, the SR system mainly focuses on the primary transmission, and thus RIS can use the signal coming from PTx to achieve its information transmission. But in the high Γ_c
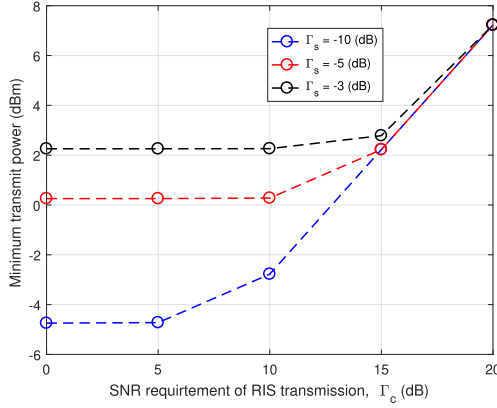
Fig. 5. Power versus SNR requirement of RIS transmission Γ_c: Number of reflecting elements $N = 20$, spreading gain $K = 100$.
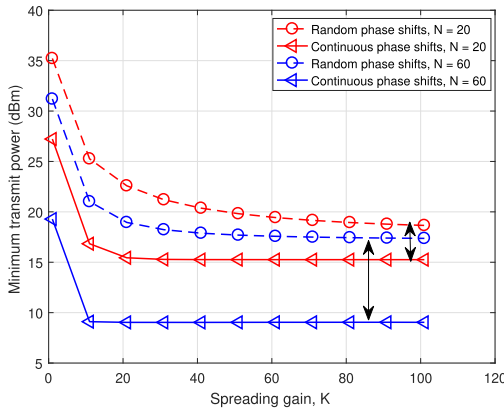

Fig. 6. Power versus spreading gain K: Number of reflecting elements $N = 20$, primary transmission requirement $\Gamma_s = 10$ dB, RIS transmission requirement $\Gamma_c = 20$ dB.
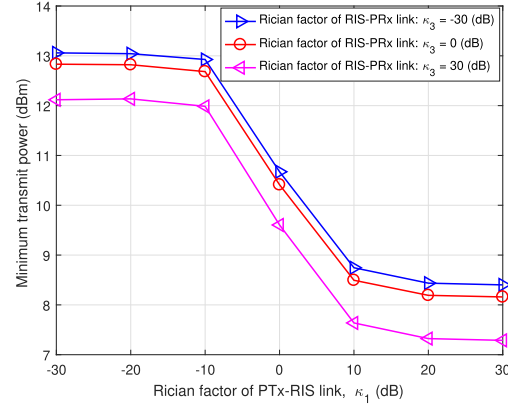

Fig. 7. Power versus Rician factors: Primary transmission requirement $\Gamma_s = 20$ dB, RIS transmission requirement $\Gamma_c = 5$ dB, number of reflecting elements $N = 20$, spreading gain $K = 100$.
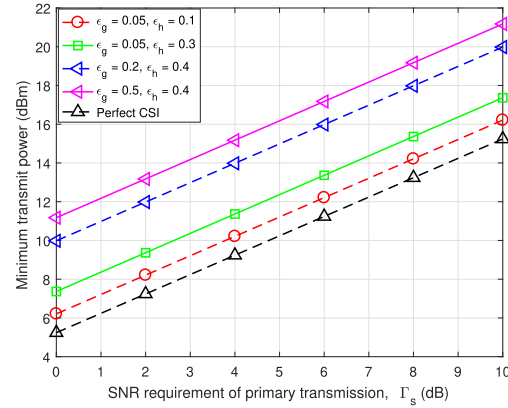

Fig. 8. Power versus uncertainty ratios, ϵ_g and ϵ_h: SIC factor $\delta = 0.01$, number of reflecting elements $N = 20$, RIS transmission requirement $\Gamma_c = 5$ dB, spreading gain $K = 100$.

regime, RIS transmission dominates the power consumption. In this case, the transmit power remains the same for different Γ_s.

Next, we investigate the relationship between the transmit power and the spreading gain (i.e., K) in Fig. 6. From (63), when the second term is greater than the first one, i.e., $\frac{\sigma^2 \Gamma_c}{K |\boldsymbol{g}^H \boldsymbol{\Theta} \boldsymbol{H} \overline{\boldsymbol{w}}|^2} \geq \frac{\sigma^2 \Gamma_s}{|\boldsymbol{h}^H \overline{\boldsymbol{w}}|^2 + |\boldsymbol{g}^H \boldsymbol{\Theta} \boldsymbol{H} \overline{\boldsymbol{w}}|^2}$, the power depends on the second term. By increasing K, the transmit power can be reduced. As K increases, the second term will be less than the first one, and thus the power now depends on the first term, resulting in a constant value regardless of K. In this case, the power $p = \frac{\sigma^2 \Gamma_s}{|\boldsymbol{h}^H \overline{\boldsymbol{w}}|^2 + |\boldsymbol{g}^H \boldsymbol{\Theta} \boldsymbol{H} \overline{\boldsymbol{w}}|^2}$, which depends on the phase shifts design. Obviously, the gap of transmit power p under the continuous and random phase shifts design increases with the number of reflecting elements N, since a larger N enables a greater passive beamforming gain, and the less transmit power is thus achieved. From Fig. 6, when $N = 20$, the continuous and random phase shifts design show almost the similar power for larger K, a trade-off between K and phase shifts design is observed. We can either use a larger K with random phase shifts design or use a smaller K with continuous phase shifts design to achieve a given power. When $N = 60$, the power gap under the two design schemes increases, and the above trade-off doesn't exist. No matter how we adjust the K, the achieved minimum power

with random phase shifts design is limited. Thus, we need to perform continuous phase shifts design to further decrease the power.

As shown in Fig. 7, it is observed that the power decreases with the Rician factor of PTx-RIS link κ_1. This can be explained as follows, when $\kappa_1 = -30\,(\text{dB})$, the PTx-RIS channel is almost Rayleigh fading, leading to a more random channel environment. Thus, more power is needed to compensate for the randomness. As κ_1 becomes larger, the PTx-RIS channel is gradually dominated by the deterministic *line-of-sight* (LoS) component, and the transmit power will decrease as the randomness decreases. Moreover, when we fix the Rician factor κ_1 to see the impact of Rician factor κ_3, similar observations can be obtained.

B. Imperfect CSI Case

Finally, we analyze the effects of imperfect CSI and imperfect SIC on the power consumption. In Fig. 8, we fix the SIC factor $\delta = 0.01$ to study the impact of imperfect CSI by varying the channel uncertainty ratios, i.e., ϵ_g and ϵ_h. It is observed that when we fix one of the uncertainty ratios and vary the other, the transmit power will increase correspondingly to make sure that the SNR requirements are satisfied for all possible channel
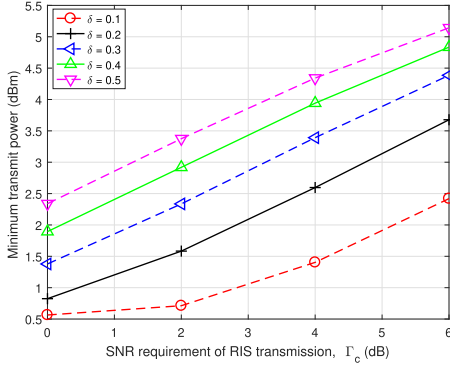
Fig. 9.　Power versus SIC factor, δ: uncertainty ratio $\epsilon_g = 0.01$, $\epsilon_h = 0.05$, number of reflecting elements $N = 20$, spreading gain $K = 100$, primary transmision requirement $\Gamma_s = -10$ dB.

errors. This observation demonstrates that perfect CSI is a prerequisite to unlock the full potential of joint beamforming. Then, in Fig. 9, we investigate the influence of imperfect SIC by fixing the uncertainty ratio $\epsilon_g = 0.01$ and $\epsilon_h = 0.05$. We can observe that power consumption increases with the increasing of SIC factor δ. This is as expected since a larger imperfect SIC will lead to the larger residual interference. Therefore, the SNR of the RIS transmission will be reduced. When the RIS transmission requirement dominates the transmit power. To guarantee the RIS transmission requirement, the PTx needs more power to alleviate the impact of imperfect SIC.

VI. CONCLUSION

In this paper, we have studied a cooperative beamforming scheme for the transmit power minimization problem in a RIS-assisted SR system, where the active transmit beamforming at the PTx and the passive reflecting beamforming at the RIS have been jointly optimized. We have first investigated the problem under the perfect CSI assumption. Particularly, we have considered both continuous and discrete phase shift setups of the RIS. Then, to make our problem more practical, we have re-investigated these cooperative beamforming problems under the imperfect CSI and the imperfect SIC assumption. Numerical results have shown that the effectiveness of the RIS information transfer and the introduction of RIS into the SR system can significantly improve the performance.

APPENDIX A
PROOF OF PROPOSITION 2

The Lagrangian function of P1-A2 can be written as

$$\mathcal{L}(\boldsymbol{A}, \lambda, \mu, \boldsymbol{Z}) = \mathrm{tr}(\boldsymbol{D}^H \boldsymbol{D} \boldsymbol{A}) - \lambda \left(\mathrm{tr}(\boldsymbol{S}_1 \boldsymbol{A}) + \mathrm{tr}(\boldsymbol{S}_2 \boldsymbol{A}) - 2\sigma^2 \Gamma_s\right)$$
$$- \mu \left(\mathrm{tr}(\boldsymbol{S}_3 \boldsymbol{A}) - \frac{1}{K}\sigma^2 \Gamma_c\right) - \mathrm{tr}(\boldsymbol{Z} \boldsymbol{A}), \tag{64}$$

where λ, μ, $\boldsymbol{Z}$ are the Lagrangian multipliers associated with constraints (24b), (24c) and (24d), respectively. Since P1-A2 is a SDP problem and thus convex with respect to $\boldsymbol{A}$, it can be verified that P1-A2 satisfies Slater's condition [42], and thus the

duality gap is zero. The optimal solution needs to satisfy the following *Karush-Kuhn-Tucher* (KKT) conditions

$$\frac{\partial \mathcal{L}(\boldsymbol{A}, \lambda, \mu, \boldsymbol{Z})}{\partial \boldsymbol{A}} = \boldsymbol{D}^H \boldsymbol{D} - \lambda(\boldsymbol{S}_1 + \boldsymbol{S}_2) - \mu \boldsymbol{S}_3 - \boldsymbol{Z} = 0, \tag{65}$$

$$\boldsymbol{Z}\boldsymbol{A} = \boldsymbol{0}, \tag{66}$$

$$\mathrm{tr}(\boldsymbol{S}_1 \boldsymbol{A}) + \mathrm{tr}(\boldsymbol{S}_2 \boldsymbol{A}) \geq 2\sigma^2 \Gamma_s, \mathrm{tr}(\boldsymbol{S}_3 \boldsymbol{A}) \geq \frac{1}{K}\sigma^2 \Gamma_c, \tag{67}$$

$$\lambda \left(\mathrm{tr}(\boldsymbol{S}_1 \boldsymbol{A}) + \mathrm{tr}(\boldsymbol{S}_2 \boldsymbol{A}) - 2\sigma^2 \Gamma_s\right) = 0, \tag{68}$$

$$\mu \left(\mathrm{tr}(\boldsymbol{S}_3 \boldsymbol{A}) - \frac{1}{K}\sigma^2 \Gamma_c\right) = 0, \tag{69}$$

$$\lambda \geq 0, \mu \geq 0, \boldsymbol{A} \succeq 0, \boldsymbol{Z} \succeq 0. \tag{70}$$

From (67), we know that rank$(\boldsymbol{A}) \geq 1$, otherwise, the inequality in (67) does not holds. Further, we have the following inequality

$$\mathrm{rank}(\boldsymbol{Z}) \overset{a}{\leq} \mathrm{rank}(\boldsymbol{Z}\boldsymbol{A}) + 2 - \mathrm{rank}(\boldsymbol{A}) \overset{b}{\leq} 1, \tag{71}$$

where "a" follows from the fact that rank$(\boldsymbol{XY}) \geq$ rank$(\boldsymbol{X}) +$ rank$(\boldsymbol{Y}) - n$, for arbitrary matrix $\boldsymbol{X}_{m \times n}$ and matrix $\boldsymbol{Y}_{n \times p}$, and "$b$" holds since rank$(\boldsymbol{Z}\boldsymbol{A}) = 0$ and rank$(\boldsymbol{A}) \geq 1$.

On the other hand, we can obtain

$$\mathrm{rank}(\boldsymbol{Z}) = \mathrm{rank}(\boldsymbol{D}^H \boldsymbol{D} - \lambda(\boldsymbol{S}_1 + \boldsymbol{S}_2) - \mu \boldsymbol{S}_3) \tag{72}$$

$$\overset{c}{\geq} \mathrm{rank}(\boldsymbol{D}^H \boldsymbol{D}) - \mathrm{rank}(\lambda(\boldsymbol{S}_1 + \boldsymbol{S}_2) + \mu \boldsymbol{S}_3) \tag{73}$$

$$\overset{d}{\geq} 2 - 1 = 1, \tag{74}$$

where "c" follows from the fact that rank$(\boldsymbol{X} - \boldsymbol{Y}) \geq$ rank$(\boldsymbol{X})$ $-$ rank$(\boldsymbol{Y})$ for any two matrices with the same dimensions. Besides, "d" holds due to that rank$(\boldsymbol{D}^H \boldsymbol{D}) =$ rank$(\boldsymbol{D}) = 2$ and rank$(\lambda(\boldsymbol{S}_1 + \boldsymbol{S}_2) + \mu \boldsymbol{S}_3) \leq 1$ since there exists at least one strictly positive between λ and μ. This can be proved by contradiction. Supposing that $\lambda = \mu = 0$, substitute this condition into (65), we can obtain $\boldsymbol{Z} = \boldsymbol{D}^H \boldsymbol{D}$. Then according to (66), we have $\boldsymbol{D}^H \boldsymbol{D} \boldsymbol{A} = \boldsymbol{0}$, implying $\boldsymbol{A} = 0$ since $\boldsymbol{D}^H \boldsymbol{D}$ is an invertible matrix. However, this result contradicts with (67). Therefore, λ and μ can not be zero simultaneously.

Combining (71) and (74), we have rank$(\boldsymbol{Z}) = 1$. Similar to (71), it follows that

$$\mathrm{rank}(\boldsymbol{A}) \leq \mathrm{rank}(\boldsymbol{Z}\boldsymbol{A}) + 2 - \mathrm{rank}(\boldsymbol{Z}) = 1. \tag{75}$$

Accordingly, it follows that rank$(\boldsymbol{A}) = 1$, and the proof of Proposition 2 is thus completed.

REFERENCES

[1] H. Zhou, Y.-C. Liang, X. Kang, and S. Sun, "Cooperative beamforming for large intelligent surface assisted symbiotic radios," in *Proc. IEEE GLOBECOM Conf.*, 2020, pp. 1–6.

[2] X. You et al., "Towards 6G wireless communication networks: Vision, enabling technologies, and new paradigm shifts," *Sci. China Inf. Sci.*, vol. 64, no. 1, pp. 1–74, 2021.

[3] L. Zhang, Y.-C. Liang, and D. Niyato, "6G visions: Mobile ultra-broadband, super internet-of-things, and artificial intelligence," *China Commun.*, vol. 16, no. 8, pp. 1–14, Aug. 2019.

[4] S. Chen, Y.-C. Liang, S. Sun, S. Kang, W. Cheng, and M. Peng, "Vision, requirements, and technology trend of 6G: How to tackle the challenges of system coverage, capacity, user data-rate and movement speed," *IEEE Wireless Commun.*, vol. 27, no. 2, pp. 218–228, Apr. 2020.

[5] Y. C. Liang, Q. Zhang, E. G. Larsson, and G. Y. Li, "Symbiotic radio: Cognitive backscattering communications for future wireless networks," *IEEE Trans. Cogn. Commun. Netw.*, vol. 6, no. 4, pp. 1242–1255, Dec. 2020.

[6] X. Kang, Y.-C. Liang, and J. Yang, "Riding on the primary: A new spectrum sharing paradigm for wireless-powered IoT devices," *IEEE Trans. Wireless Commun.*, vol. 17, no. 9, pp. 6335–6347, Sep. 2018.

[7] R. Long, Y.-C. Liang, H. Guo, G. Yang, and R. Zhang, "Symbiotic radio: A new communication paradigm for passive internet-of-things," *IEEE Internet Things J.*, vol. 7, no. 2, pp. 1350–1363, Feb. 2020.

[8] H. Guo, Y.-C. Liang, R. Long, S. Xiao, and Q. Zhang, "Resource allocation for symbiotic radio system with fading channels," *IEEE Access*, vol. 7, pp. 34333–34347, 2019.

[9] Q. Wu and R. Zhang, "Towards smart and reconfigurable environment: Intelligent reflecting surface aided wireless network," *IEEE Commun. Mag.*, vol. 58, no. 1, pp. 106–112, Jan. 2020.

[10] Y. C. Liang, R. Long, Q. Zhang, J. Chen, H. V. Cheng, and H. Guo, "Large intelligent surface/antennas (LISA): Making reflective radios smart," *J. Commun. Inf. Netw.*, vol. 4, no. 2, pp. 40–50, Jun. 2019.

[11] C. Huang et al., "Holographic MIMO surfaces for 6G wireless networks: Opportunities, challenges, and trends," *IEEE Wireless Commun.*, vol. 27, no. 5, pp. 118–125, Oct. 2020.

[12] M. Di Renzo et al., "Smart radio environments empowered by reconfigurable intelligent surfaces: How it works, state of research, and the road ahead," *IEEE J. Sel. Areas Commun.*, vol. 38, no. 11, pp. 2450–2525, Nov. 2020.

[13] M. Di Renzo et al., "Smart radio environments empowered by reconfigurable ai meta-surfaces: An idea whose time has come," *EURASIP J. Wireless Commun. Netw.*, vol. 20 19, no. 1, pp. 1–20, 2019.

[14] Q. Wu and R. Zhang, "Intelligent reflecting surface enhanced wireless network via joint active and passive beamforming," *IEEE Trans. Wireless Commun.*, vol. 18, no. 11, pp. 5394–5409, Nov. 2019.

[15] Q. Wu and R. Zhang, "Beamforming optimization for wireless network aided by intelligent reflecting surface with discrete phase shifts," *IEEE Trans. Commun.*, vol. 68, no. 3, pp. 1838–1851, Mar. 2020.

[16] H. Guo, Y.-C. Liang, J. Chen, and E. G. Larsson, "Weighted sum-rate maximization for reconfigurable intelligent surface aided wireless networks," *IEEE Trans. Wireless Commun.*, vol. 19, no. 5, pp. 3064–3076, May 2020.

[17] J. Chen, Y.-C. Liang, Y. Pei, and H. Guo, "Intelligent reflecting surface: A programmable wireless environment for physical layer security," *IEEE Access*, vol. 7, pp. 82599–82612, 2019.

[18] Z. He and X. Yuan, "Cascaded channel estimation for large intelligent metasurface assisted massive MIMO," *IEEE Wireless Commun. Lett.*, vol. 9, no. 2, pp. 210–214, Feb. 2020.

[19] C. Hu, L. Dai, S. Han, and X. Wang, "Two-timescale channel estimation for reconfigurable intelligent surface aided wireless communications," *IEEE Trans. Commun.*, vol. 69, no. 11, pp. 7736–7747, Nov. 2021.

[20] L. Wei, C. Huang, G. C. Alexandropoulos, C. Yuen, Z. Zhang, and M. Debbah, "Channel estimation for RIS-empowered multi-user MISO wireless communications," *IEEE Trans. Commun.*, vol. 69, no. 6, pp. 4144–4157, Jun. 2021.

[21] G. Zhou, C. Pan, H. Ren, K. Wang, and A. Nallanathan, "A framework of robust transmission design for IRS-aided MISO communications with imperfect cascaded channels," *IEEE Trans. Signal Process.*, vol. 68, pp. 5092–5106, 2020, doi: 10.1109/TSP.2020.3019666.

[22] J. Wang, Y.-C. Liang, S. Han, and Y. Pei, "Robust beamforming and phase shift design for IRS-enhanced multi-user MISO downlink communication," in *Proc. IEEE Int. Conf. Commun.*, 2020, pp. 1–6.

[23] X. Yu, D. Xu, Y. Sun, D. W. K. Ng, and R. Schober, "Robust and secure wireless communications via intelligent reflecting surfaces," *IEEE J. Sel. Areas Commun.*, vol. 38, no. 11, pp. 2637–2652, Nov. 2020.

[24] S. Li, B. Duo, M. D. Renzo, M. Tao, and X. Yuan, "Robust secure UAV communications with the aid of reconfigurable intelligent surfaces," *IEEE Trans. Wireless Commun.*, vol. 20, no. 10, pp. 6402–6417, Oct. 2021.

[25] L. Zhang, C. Pan, Y. Wang, H. Ren, and K. Wang, "Robust beamforming design for intelligent reflecting surface aided cognitive radio systems with imperfect cascaded CSI," *IEEE Trans. Cogn. Commun. Netw.*, vol. 8, no. 1, pp. 186–201, Mar. 2022.

[26] M. Hua, Q. Wu, L. Yang, R. Schober, and H. V. Poor, "A novel wireless communication paradigm for intelligent reflecting surface based symbiotic radio systems," *IEEE Trans. Signal Process.*, vol. 70, pp. 550–565, 2022, doi: 10.1109/TSP.2021.3135603.

[27] J. Hu, Y.-C. Liang, and Y. Pei, "Reconfigurable intelligent surface enhanced multi-user MISO symbiotic radio system," *IEEE Trans. Commun.*, vol. 69, no. 4, pp. 2359–2371, Apr. 2021.

[28] C. Wang, Z. Li, T.-X. Zheng, D. W. K. Ng, and N. Al-Dhahir, "Intelligent reflecting surface-aided secure broadcasting in millimeter wave symbiotic radio networks," *IEEE Trans. Veh. Technol.*, vol. 70, no. 10, pp. 11050–11055, Oct. 2021.

[29] X. Chen, R. Jia, and D. W. K. Ng, "On the design of massive non-orthogonal multiple access with imperfect successive interference cancellation," *IEEE Trans. Commun.*, vol. 67, no. 3, pp. 2539–2551, Mar. 2019.

[30] G. Im and J. H. Lee, "Outage probability for cooperative NOMA systems with imperfect SIC in cognitive radio networks," *IEEE Commun. Lett.*, vol. 23, no. 4, pp. 692–695, Apr. 2019.

[31] Q. Wu, S. Zhang, B. Zheng, C. You, and R. Zhang, "Intelligent reflecting surface-aided wireless communications: A tutorial," *IEEE Trans. Commun.*, vol. 69, no. 5, pp. 3313–3351, May 2021.

[32] B. Di, H. Zhang, L. Li, L. Song, Y. Li, and Z. Han, "Practical hybrid beamforming with finite-resolution phase shifters for reconfigurable intelligent surface based multi-user communications," *IEEE Trans. Veh. Technol.*, vol. 69, no. 4, pp. 4565–4570, Apr. 2020.

[33] H. Liu, X. Yuan, and Y. J. A. Zhang, "Matrix-calibration-based cascaded channel estimation for reconfigurable intelligent surface assisted multiuser MIMO," *IEEE J. Sel. Areas Commun.*, vol. 38, no. 11, pp. 2621–2636, Nov. 2020.

[34] G. Yang, Y.-C. Liang, R. Zhang, and Y. Pei, "Modulation in the air: Backscatter communication over ambient OFDM carrier," *IEEE Trans. Commun.*, vol. 66, no. 3, pp. 1219–1233, Mar. 2018.

[35] H. Sun, B. Xie, R. Q. Hu, and G. Wu, "Non-orthogonal multiple access with SIC error propagation in downlink wireless MIMO networks," in *Proc. IEEE Veh. Technol. Conf.*, 2016, pp. 1–5.

[36] S. R. Islam, N. Avazov, O. A. Dobre, and K.-S. Kwak, "Power-domain non-orthogonal multiple access (NOMA) in 5G systems: Potentials and challenges," *IEEE Commun. Surveys Tuts.*, vol. 19, no. 2, pp. 721–742, Apr.–Jun. 2017.

[37] T. L. Jensen and E. De Carvalho, "An optimal channel estimation scheme for intelligent reflecting surfaces based on a minimum variance unbiased estimator," in *Proc. IEEE Int. Conf. Acoust., Speech, Signal Process.*, 2020, pp. 5000–5004.

[38] K.-Y. Wang, A. M.-C. So, T.-H. Chang, W.-K. Ma, and C.-Y. Chi, "Outage constrained robust transmit optimization for multiuser MISO downlinks: Tractable approximations by conic optimization," *IEEE Trans. Signal Process.*, vol. 62, no. 21, pp. 5690–5705, Sep. 2014.

[39] P.-J. Chung, H. Du, and J. Gondzio, "A probabilistic constraint approach for robust transmit beamforming with imperfect channel information," *IEEE Trans. Signal Process.*, vol. 59, no. 6, pp. 2773–2782, Jun. 2011.

[40] G. Zheng, K.-K. Wong, and T.-S. Ng, "Robust linear MIMO in the downlink: A worst-case optimization with ellipsoidal uncertainty regions," *EURASIP J. Adv. Signal Process.*, vol. 2008, pp. 1–15, 2008.

[41] Q. Li and W.-K. Ma, "Optimal and robust transmit designs for MISO channel secrecy by semidefinite programming," *IEEE Trans. Signal Process.*, vol. 59, no. 8, pp. 3799–3812, Aug. 2011.

[42] M. Grant and S. Boyd, "CVX: Matlab software for disciplined convex programming, version 2.2," Jan. 2020. [Online]. Available: http://cvxr.com/cvx

[43] Z. Luo, W. Ma, A. M. So, Y. Ye, and S. Zhang, "Semidefinite relaxation of quadratic optimization problems," *IEEE Signal Process. Mag.*, vol. 27, no. 3, pp. 20–34, May 2010.

[44] W. Wu et al., "Dynamic RAN slicing for service-oriented vehicular networks via constrained learning," *IEEE J. Sel. Areas Commun.*, vol. 39, no. 7, pp. 2076–2089, Jul. 2021.

[45] "Technical specification group radio access network; study on 3D channel model for LTE (release 12)," 3GPP, Sophia Antipolis Cedex, France, TR 36.873 V12.7.0, Dec. 2017.

Hu Zhou (Graduate Student Member, IEEE) received the B.S. degree in communication engineering in 2020 from the University of Electronic Science and Technology of China, where he is currently working toward the Ph.D. degree. His research interests include symbiotic radio, reconfigurable intelligent surface, backscatter communication, and Internet-of-Things.
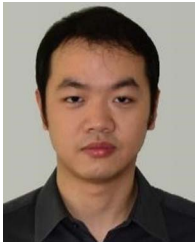
Xin Kang (Senior Member, IEEE) received the B. Eng. degree in electrical engineering from Xi'an Jiaotong University, Xi'an, China, in 2005 and the Ph.D. degree in electrical and computer engineering from the National University of Singapore, Singapore, in 2011. From 2011 to 2014, he was a Research Scientist with the Institute for Infocomm Research, A*STAR, Singapore. After that, he joined Shield Lab, Huawei Singapore Research Center as a Senior Researcher. In 2016, he joined the University of Electronic Science and Technology of China, Chengdu, China, as an Honorary Professor. He has more than 15 years research experience and his research interests include optimization, wireless communications, network security, machine-learning based trust modeling, digital identity and privacy, game theory, blockchain, and security protocol design. He has authored or coauthored more than 70 IEEE top journal and conference papers, and more than ten of them are listed as SCI highly cited research papers. He was the recipient of Best Paper Award from IEEE ICC, 2017, and 50 best paper awards from IEEE GlobeCom, 2014. After joining Huawei, he has filed more than 40 patents on security protocol designs. Besides, he is also very active in standardization. Till now, he has filed more than 50 patents, and contributed more than 30 technical proposals to 3GPP SA3. He is one of key contributors to the newly published ITU-T standard X.1365, and the on-going work item X.ztd-iot. He is also one of the key contributors to Huawei 5G security white paper series.

Sumei Sun (Fellow, IEEE) is currently the Principal Scientist, Deputy Executive Director (Research), and Head of the Communications and Networks Department with the Institute for Infocomm Research, Singapore. She is holding a joint appointment with the Singapore Institute of Technology, Singapore, and an adjunct appointment with the National University of Singapore, Singapore, both as a full professor. Her current research interests include next-generation wireless communications, joint sensing-communication-computing-control design, and industrial Internet of Things. She is the Editor-in-Chief of IEEE OPEN JOURNAL OF VEHICULAR TECHNOLOGY, Steering Committee Chair for IEEE TRANSACTIONS ON MACHINE LEARNING IN COMMUNICATIONS AND NETWORKS, a Distinguished Speaker of the IEEE Vehicular Technology Society 2018–2024, a Member-at-Large with the IEEE Communications Society (2021–2023), and a Member of IEEE Vehicular Technology Society Board of Governors (2022–2024).

Ying-Chang Liang (Fellow, IEEE) was a Professor with The University of Sydney, Sydney, NSW, Australia, the Principal Scientist and Technical Advisor with the Institute for Infocomm Research, Singapore, and a Visiting Scholar with Stanford University, Stanford, CA, USA. He is currently a Professor with the University of Electronic Science and Technology of China, Chengdu, China, where he leads the Center for Intelligent Networking and Communications. His research interests include wireless networking and communications, cognitive radio, symbiotic communications, dynamic spectrum access, the Internet of Things, artificial intelligence, and machine learning techniques.

Dr. Liang is also a Foreign Member of the Academia Europaea. He has been recognized by Thomson Reuters, now Clarivate Analytics as a Highly Cited Researcher since 2014. He was the recipient of Prestigious Engineering Achievement Award from The Institution of Engineers, Singapore, in 2007, the Outstanding Contribution Appreciation Award from the IEEE Standards Association, in 2011, and the Recognition Award from the IEEE Communications Society Technical Committee on Cognitive Networks, in 2018. He was also the recipient of numerous paper awards, including the IEEE Communications Society Advances in Communication Prize Paper Award, in 2022, IEEE Communications Society Stephen O. Rice Prize in 2021, and IEEE Vehicular Technology Society Jack Neubauer Memorial Award, in 2014. He was the Chair of the IEEE Communications Society Technical Committee on Cognitive Networks. He was the TPC Chair and the Executive Co-Chair of the IEEE Globecom17. He was a Guest/Associate Editor for the IEEE TRANSACTIONS ON WIRELESS COMMUNICATIONS, the IEEE JOURNAL ON SELECTED AREAS IN COMMUNICATIONS, the IEEE Signal Processing Maga-zine, the IEEE TRANSACTIONS ON VEHICULAR TECHNOLOGY, and the IEEE TRANSACTIONS ON SIGNAL AND INFORMATION PROCESSING OVER NETWORKS. He was an Associate Editor-in-Chief for the Random Matrices: Theory and Applications (World Scientific). He is also the Founding Editor-in-Chief of the IEEE JOURNAL ON SELECTED AREAS IN COMMUNICATIONS: COGNITIVE RADIO SERIES and the Key Founder and the Editor-in-Chief for the IEEE TRANSACTIONS ON COGNITIVE COMMUNICATIONS AND NETWORKING. He is also an Associate Editor-in-Chief for *China Communications*. He was a Distinguished Lecturer of the IEEE Communications Society and the IEEE Vehicular Technology Society.

Xuemin Shen (Fellow, IEEE) received the Ph.D. degree in electrical engineering from Rutgers University, New Brunswick, NJ, USA, in 1990. He is currently a University Professor with the Department of Electrical and Computer Engineering, University of Waterloo, ON, Canada. His research interests include network resource management, wireless network security, Internet of Things, 5G and beyond, and vehicular networks. Dr. Shen was the recipient of the Canadian Award for Telecommunications Research from the Canadian Society of Information Theory, in 2021, R.A. Fessenden Award, from IEEE, Canada, in 2019, Award of Merit from the Federation with Chinese Canadian Professionals, Ontario, in 2019, James Evans Avant Garde Award from the IEEE Vehicular Technology Society, in 2018, Joseph LoCicero Award, in 2015, and Education Award from the IEEE Communications Society (ComSoc), in 2017, and Technical Recognition Award from Wireless Communications Technical Committee, in 2019, and AHSN Technical Committee, in 2013. He was also the recipient of the Excellent Graduate Supervision Award from the University of Waterloo, in 2006, and Premiers Research Excellence Award from the Province of Ontario, Canada, in 2003. He is a registered Professional Engineer of Ontario, Canada, an Engineering Institute of Canada Fellow, a Canadian Academy of Engineering Fellow, Royal Society of Canada Fellow, Chinese Academy of Engineering Foreign Member, and Distinguished Lecturer of the IEEE Vehicular Technology Society and Communications Society.

He was the Technical Program Committee Chair/Co-Chair of IEEE Globecom16, IEEE Infocom14, IEEE VTC10 Fall, and IEEE Globecom07, and the Chair of the IEEE ComSoc Technical Committee on Wireless Communications. He is the President for the IEEE ComSoc. He was the Vice President of Technical & Educational Activities, Vice President of Publications, Member-at-Large on the Board of Governors, Chair of the Distinguished Lecturer Selection Committee, and Member of IEEE Fellow Selection Committee of the ComSoc. He was the Editor-in-Chief of the IEEE IoT JOURNAL, IEEE NETWORK, and *IET Communications*.